

## Weight Consistency Specifies Regularities of Macaque Cortical Networks

N. T. Markov<sup>1,2</sup>, P. Misery<sup>1,2</sup>, A. Falchier<sup>1,2,5</sup>, C. Lamy<sup>1,2</sup>, J. Vezoli<sup>1,2</sup>, R. Quilodran<sup>1,2</sup>, M. A. Gariel<sup>1,2</sup>, P. Giroud<sup>1,2</sup>, M. Ercsey-Ravasz<sup>3</sup>, L. J. Pilaz<sup>1,2</sup>, C. Huissoud<sup>1,2</sup>, P. Barone<sup>1,2,6</sup>, C. Dehay<sup>1,2</sup>, Z. Toroczkai<sup>3</sup>, D. C. Van Essen<sup>4</sup>, H. Kennedy<sup>1,2</sup> and K. Knoblauch<sup>1,2</sup>

<sup>1</sup>Stem cell and Brain Research Institute, Institut National de la Sante et de la Recherche Medicale U846, 69500 Bron, France, <sup>2</sup>Université de Lyon, Université Lyon I, 69003 Lyon, France, <sup>3</sup>Department of Physics, Interdisciplinary Center for Network Science and Applications, University of Notre Dame, Notre Dame, IN 46556, USA, <sup>4</sup>Department of Anatomy and Neurobiology, Washington University School of Medicine, St Louis, MO 63110, USA

<sup>5</sup>Current address: Cognitive Neuroscience and Schizophrenia Program, Nathan S. Kline Institute for Psychiatric Research, Orangeburg, NY 10962, USA

<sup>6</sup>Cerveau et Cognition, UMR 5549, 31062 Toulouse cedex, France

Markov and Misery have contributed equally to this work

Address correspondence to Dr H. Kennedy, Stem cell and brain research institute, Institut National de la Sante et de la Recherche Medicale U846, 18 avenue du Doyen Lepine, 69500 Bron, France. Email: henry.kennedy@inserm.fr.

**To what extent cortical pathways show significant weight differences and whether these differences are consistent across animals (thereby comprising robust connectivity profiles) is an important and unresolved neuroanatomical issue. Here we report a quantitative retrograde tracer analysis in the cynomolgus macaque monkey of the weight consistency of the afferents of cortical areas across brains via calculation of a weight index (fraction of labeled neurons, FLN). Injection in 8 cortical areas (3 occipital plus 5 in the other lobes) revealed a consistent pattern: small subcortical input (1.3% cumulative FLN), high local intrinsic connectivity (80% FLN), high-input from neighboring areas (15% cumulative FLN), and weak long-range corticocortical connectivity (3% cumulative FLN). Corticocortical FLN values of projections to areas V1, V2, and V4 showed heavy-tailed, lognormal distributions spanning 5 orders of magnitude that were consistent, demonstrating significant connectivity profiles. These results indicate that 1) connection weight heterogeneity plays an important role in determining cortical network specificity, 2) high investment in local projections highlights the importance of local processing, and 3) transmission of information across multiple hierarchy levels mainly involves pathways having low FLN values.**

**Keywords:** amygdala, area 17, macaque, network, primate, thalamus

### Introduction

Primate cerebral cortex contains many (~100) distinct areas interconnected by several thousands of pathways (Young 1993; Kotter and Sommer 2000; Stephan et al. 2000; Van Essen 2003; Kaiser and Hilgetag 2006). The vast majority of studies provide only qualitative descriptions of the strength of various cortical pathways; few studies have used quantitative data to explore how connection weights specify cortical networks. A systematic attack on this problem is sorely needed in order to enable characterization of cortical organization and function using a growing arsenal of computational and network analysis tools newly available to neuroscientists.

The present study has 2 aims. The first is to characterize the spectrum of connection weights of pathways within an animal and establish if they exhibit significant differences. The second is to evaluate the consistency of such differences across animals. This assessment is essential for understanding the nature of cortical connectivity profiles and ultimately for

deciphering brain circuitry. Tackling these challenges requires quantification of large numbers of pathways across animals. Retrograde tracers are more suitable than anterograde tracers for such a comparative quantification study because of the relative ease of counting neurons participating in a given projection as opposed to counting synapses (Batardiere et al. 1998; Barone et al. 2000; Falchier et al. 2002; Vezoli et al. 2004). In the present study, largely centered on the visual system, we have examined 2 general aspects of cortical connectivity. The first concerns the relative weight of local connections versus long-distance connections from other cortical areas and subcortical structures. The second concerns the distribution of connection weights between cortical areas and their variability across animals.

The relative weight of local versus subcortical inputs is intimately linked to our understanding of how information is extracted by the cortex from its thalamic input. Thalamic input to area V1 is thought to interact with local circuits to generate the receptive field properties of cortical neurons (Douglas and Martin 1991; Wang et al. 2010). The thalamus contributes only a small proportion of synapses to area V1 (1–2%); the majority of synapses originate from the recurrent local circuitry that allows signal amplification and refinement (Latawiec et al. 2000; da Costa and Martin 2009). However, the relative contribution of intrinsic versus long-distance interareal connections to the local synaptic pool remains uncertain (Binzegger et al. 2004, 2007; Stepanyants et al. 2009). Because the number of synapses contributed by a given axon can vary over a wide range, data at the synapse level do not allow direct inferences about connection weight in terms of neuronal numbers. The latter is important for incorporating local, long-distance, and subcortical interactions into models of cortical function.

The distribution and weights of connections between cortical areas are related to theories of cortical processing. Information flows through the cortex via a complex network of corticocortical connections that play a crucial role in shaping the functional specializations of cortical areas (Rockland and Pandya 1981; Boussaoud et al. 1990; Felleman and Van Essen 1991; Kaas and Collins 2001). Previous efforts to understand this network have emphasized binary aspects of interareal connectivity (connected vs. not connected). Working with a database of 32 visual areas, Felleman and Van Essen (1991) estimated a connection density of 30–45% (i.e., of the total possible connections, there was evidence that 30–45% actually

exist). The high density of the cortical matrix means that the presence or absence of a given cortical pathway (i.e., a binary analysis) can provide only limited insights into the specificity of cortical networks.

Important aspects of cortical network specificity and function must in some way depend heavily on differences in connection weights of various pathways. The paucity of corticocortical connectivity studies reporting quantitative neuroanatomical data largely reflects the difficulty in accurately quantifying the weight of connections between cortical areas. The motivation to pursue such analyses has been dampened by evidence that the connection weight of any given pathway is highly variable or overdispersed with a >100-fold range (Musil and Olson 1988a, 1988b; Olson and Musil 1992; MacNeil et al. 1997; Scannell et al. 2000). However, these reports examining the consistency of connection weights largely relied on data compilations across laboratories, often from studies using different tracing techniques and definitions of areas; these factors may contribute to the observed overdispersion (Scannell et al. 2000). Here, we used tracing strategies that minimize methodological variability, analyzed results from 16 injections in 8 cortical areas, and developed a quantitative database of connection weights. Armed with this database, we have explored statistical approaches that permit appropriate treatment of the issue of overdispersion.

Overdispersion in count data generally signifies that the variance exceeds the mean, thus violating the properties of a Poisson distribution. Overdispersion, in fact, occurs commonly in count data and can be attributed to any of several factors including clustering and/or correlation in the data (Hilbe 2007). Its presence need not be a hindrance to analysis, as several models exist for incorporating its effects (Lindsey 1999; Venables and Ripley 2002; Hilbe 2007). However, failure to do so results in underestimating the true variance of the data, leading to an increase in attribution of significance to differences when the hypothesis of no difference is in fact correct (a so-called Type 1 error). Thus, an important step in establishing a connectivity profile is to characterize how the data are distributed and to estimate their variability. An issue in making such estimates is that for practical reasons, only a limited number of injections can be made. Each injection, however, results in projections from over 20 areas with average strengths ranging over many orders of magnitude. This yields an adequate data set for characterizing mean/variance relations in the data.

We focused on 3 early visual areas whose connectivity has been extensively studied (Felleman and Van Essen 1991; Ungerleider et al. 1998, 2008; Barone et al. 2000; Falchier et al. 2002). These areas are large and the retinotopy is well established with respect to defined landmarks (Gattass et al. 2005). This enabled the use of published maps so as to perform injections in retinotopically clearly defined regions, thereby minimizing variability associated with the known eccentricity dependence of connectivity patterns (Falchier et al. 2002; Gattass et al. 2005; Ungerleider et al. 2008). We used 2 fluorescent tracers, fast blue (F<sub>s</sub>B) and diamidino yellow (DY), that have restricted and well-defined uptake zones that we could confine to cortex subserving central visual space (Bullier et al. 1984; Kennedy and Bullier 1985; Perkel et al. 1986; Conde 1987). The restricted uptake zone is important for enabling accurate measurements of local connectivity immediately adjacent to the uptake zone and for avoiding tracer spillage into white matter and into adjacent cortical areas.

Previously, we have shown that these tracers can reveal many pathways that had not been revealed using other tracers such as optimized horseradish peroxidase (Bullier and Kennedy 1983; Kennedy and Bullier 1985; Perkel et al. 1986; Barone et al. 2000; Falchier et al. 2002). In the present study, repeat injections in the target areas coupled with previously developed quantitative techniques (Batardiere et al. 1998; Vezoli et al. 2004) enabled us to characterize the fraction of labeled neurons (FLN) (Falchier et al. 2002) in cortical and subcortical structures. Our results indicate 3 important findings: 1) V1, V2, and V4 each receive inputs from 25 cortical areas; the consistency of each pathway can be modeled by a negative binomial distribution, indicating a predictable degree of variability; 2) The connection weights (FLN values) of the full complement of inputs to areas V1, V2, and V4 span more than 5 orders of magnitude, with a connectivity profile that conforms to a lognormal distribution; and 3) The bulk of cortical connectivity is largely local, and direct information exchange between hierarchical levels beyond immediate neighbors involves pathways originating from modest numbers of neurons. These results show that the connectivity profiles are well defined, share regular characteristics across areas, and impose important constraints on how cortical circuits are wired and how they function.

Quantitative information derived from these tracer injections provides invaluable reference data for comparisons with connectivity patterns inferred using magnetic resonance (MR)-based structural and functional imaging methods. These include tractography analyses based on diffusion imaging (Johansen-Berg and Behrens 2009) and resting-state functional connectivity (R-functional magnetic resonance imaging [fMRI]) that can be performed in monkeys (Vincent et al. 2007) and humans (Fox and Raichle 2007; Van Dijk et al. 2010). To facilitate objective comparisons using these different methods, it is important to bring the data into a common spatial framework. Here, we bring the tracer-based connectivity data into register with the macaque F99 atlas, which has previously been used for analyzing functional connectivity (Vincent et al. 2007) and as a substrate for interspecies comparisons with humans (Orban et al. 2004; Vincent et al. 2009).

## Materials and Methods

### *Surgery and Histology*

Surgical and histology procedures were in accordance with European requirements 86/609/EEC and approved by the appropriate veterinary and ethical services. The experiments were conducted on the Cynomolgus macaque (*Macaca fascicularis*). A detailed description of these methods is given elsewhere (Barone et al. 2000).

Following premedication with atropine (1.25 mg, intramuscularly [i.m.]) and dexamethasone (4 mg, i.m.), monkeys were prepared for surgery under ketamine hydrochloride (20 mg/kg, i.m.) and chlorpromazine (2 mg/kg, i.m.). Anesthesia was continued with halothane in N<sub>2</sub>O/O<sub>2</sub> (70/30). Heart rate was monitored and artificial respiration adjusted to maintain the end-tidal CO<sub>2</sub> at 4.5–6%. The rectal temperature was maintained at 37 °C. Single injections of DY and F<sub>s</sub>B (0.1–0.6 μL) were made by means of Hamilton syringes that in 4 of the 5 area V1 injections were equipped with glass pipettes (40–80 μm diameter). Injections were made at a shallow angle to the cortical surface to form longitudinal injection sites in the cortical gray matter. The cortex was penetrated to 2–3 mm and 0.1 μL of tracer injected at regular intervals as the needle was retracted. Figure 1 shows a Nissl-stained section at the level of each of the injection sites, the approximate position of the uptake zone is indicated (see

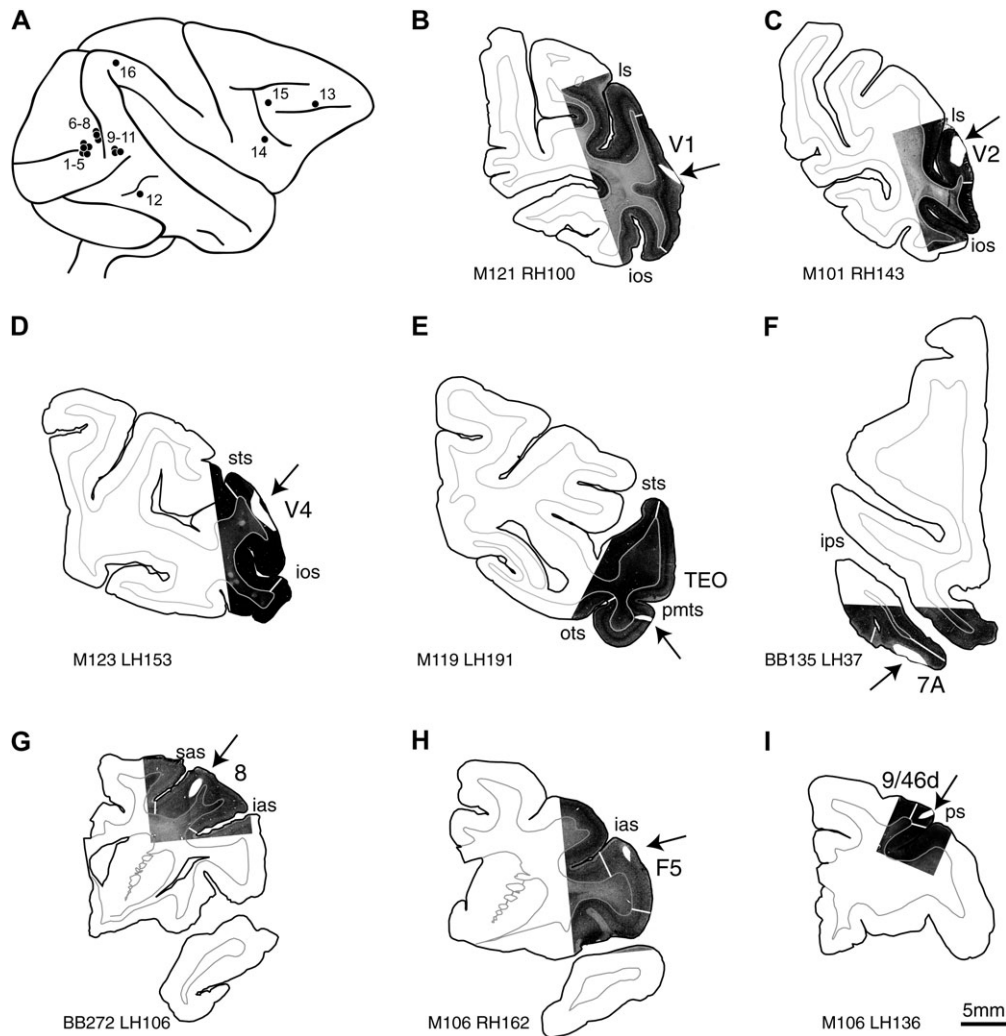


**Figure 1.** Injection sites. (A) Injection sites indicated on a lateral view of a cerebral hemisphere. For case numbers, see Table 1. (B)—(I) B: V1, (C) V2, (D) V4, (E) TEO, (F) 7A, (G) 8, (H) F5, (I) 9/46d. A plot map is overlaid on photomontage of Nissl stain (objective  $\times 10$ ) for each injection site. Sections are coronal plane except (F), which is a horizontal section. Uptake zones are indicated by arrows. Scale bar = 5 mm. Relevant sulci abbreviations are indicated and full names can be found in the abbreviation index table.

Supplementary Discussion). In one V2 injection (case M101 LH), the injection site encroached on the underlying white matter (Supplementary Fig. S7). This did not appear to influence either the FLN distribution in the cortex (Supplementary Fig. S7) or the thalamus, and this injection has been maintained in the study.

Following 11–13 days survival, animals were deeply anesthetized before being perfused with 4–8% paraformaldehyde/0.05% glutaraldehyde in phosphate buffer (0.1 M, pH 7.4). Cryoprotection was ensured by sucrose or glycerol gradient perfusions. Brains were removed and kept in the cryoprotecting liquid overnight or until sinking. Horizontal or coronal 40- $\mu$ m-thick sections were cut on a freezing microtome (Table 1). Sections at regular intervals were reacted for cytochrome oxidase and acetylcholinesterase activity (Barone et al. 2000) and sternberger monoclonals incorporated-32 (SMI-32) (Hof and Morrison 1995). Every third section was mounted on gelatinized glass slides and used to explore projection pathways.

#### Charting Labeled Neurons

The injected area is referred to as the target area and the area containing labeled neurons as the source area. The restricted region of the source area containing the labeled cells is the projection zone (Supplementary Fig. S1) (Barone et al. 2000). The uptake zone of the dye corresponds to the zone of dense extracellular label immediately surrounding the needle tract and in some cases containing necrotic

**Table 1**

List of injected animals

Case	Animal	Hemisphere	Tracers	Injection site	Plane of section
1	M81	LH	DY	V1 central	H
2	M85	LH	FB	V1 central	H
3	M85	RH	FB + DY	V1 central	H
4	M88	RH	FB	V1 central	H
5	M121	RH	DY	V1 central	C
6	M101	LH	DY	V2 central	C
7	M101	RH	FB	V2 central	C
8	M103	LH	DY	V2 central	C
9	BB187	LH	FB	V4 central	H
10	M121	RH	FB	V4 central	C
11	M123	LH	DY	V4 central	C
12	M119	LH	FB	TEO	C
13	M106	LH	FB	9/46d	C
14	M106	RH	DY	F5	C
15	BB272	LH	DY	8	C
16	BB135	LH	DY	7A	H

cells (see Discussion and Technical considerations in Supplementary information). In all cases, the uptake zone was characterized with respect to the retinotopic representation of the area injected, sampling of cortical layers, and possible involvement of white matter.

A first group of 9 animals was used for repeat injections to assess variability of FLN across animals (Table 1). These injections were made in the central representation of areas V1, V2, and V4 (Gattass et al. 2005). A second group of 4 animals was used to assess the consistency of the pattern of local, long-distance, and subcortical inputs by making injections in TEO, F5, 9/46d, 8, and 7A.

Precise charts of neuron location were made. In one V4 case (BB187), charts were made on an X-Y plotting table electronically coupled to the microscope stage (D-filter set 355–425 nm). This generates maps of labeled neurons on large sheets of paper that are subsequently matched to projections of the stained section so as to locate cortical layers and landmarks. In all remaining cases, neurons were charted using the Mercator<sup>®</sup> software package running on ExploraNova<sup>®</sup> technology. This much-improved system stores in a digital format charts of whole-brain sections with the accurate counts and coordinates of labeled neurons, making it possible to view the charted sections at different magnifications.

The curvature of cortex as well as the heterogeneity of labeling pattern in the source areas necessitated a controlled sampling and counting of neurons at close intervals throughout the projection zones. This generates density profiles that are used to calculate FLN values (Supplementary Fig. S1). Although laborious, this is crucial in order to obtain stable neuron counts that do not vary according to sampling frequency (Batardiére et al. 1998; Vezoli et al. 2004). Results from these injections are available in Supplementary Table S1.

Throughout the text, scales are as measured in the processed material and no corrections for shrinkage have been made.

### Criteria for Cortical Parcellation

It is important to use consistent criteria to distinguish different cortical areas and to be able to count neurons throughout a maximum extent of the projection zones in each area. We used histological criteria (Supplementary Figs S2–S5) as well as atlas-based landmarks to segment the cortex into distinct areas (Paxinos et al. 2000; Saleem and Logothetis 2007). We used our cytoarchitectonic criteria as well as that of others as described below to build an atlas indicating our areal limits (Supplementary Fig. S6). In many regions, there are published parcellations that differ substantially from the ones we identified here. While the choice of parcellation obviously impacts our detailed results, use of alternative parcellations would only modestly impact our main conclusions.

We have published segmentation criteria elsewhere for visual areas (Barone et al. 2000; Falchier et al. 2002) and have used reported chemoarchitectonic and cytoarchitectonic criteria (Hof and Morrison 1995; Brewer et al. 2002; Gattass et al. 2005). We used published criteria and landmarks to delineate the separation between V4 and DP (Stepniewska et al. 2005). V6 and V6A were combined into the single complex PO (Colby et al. 1988; Luppino et al. 2005). We used published criteria for prefrontal areas, and included the transitional areas 9/46d and 9/46v (Barbas and Pandya 1989; Petrides and Pandya 1999; Paxinos et al. 2000). In the dorsal bank of the superior branch of the arcuate sulcus and extending medially, we identify area 8B (Preuss and Goldman-Rakic 1991). We identified area 8 as extending over a major portion of the inferior arcuate sulcus (Barbas and Pandya 1989). In auditory cortex, we used the nomenclature and subdivisions of the Kaas group (Hackett et al. 1998; Kaas and Hackett 1998) and of Van Essen and Anderson for parietal cortex (Andersen et al. 1990; Lewis and Van Essen 2000). All insular complexes were combined into a single entity we call Insula (Ins) (Jones and Burton 1976; Mesulam and Mufson 1982). We subdivide the frontal cortex in areas F1–F7 (Luppino and Rizzolatti 2000). In the superior bank of the STS, we defined STP as including cytoarchitectonic areas TAA and TPO based on published criteria using SMI-32 immunoreactivity (Padberg et al. 2003). In the fundus of STS rostral to FST and MST, we identify areas PGa and IPa (Seltzer and Pandya 1978). All subdivisions of area TE were combined into a single complex that shares borders with the perirhinal (PERIRHINAL) and parahippocampal (TH/TF) cortices (Suzuki and Amaral 2003; Saleem et al. 2007). The entorhinal (ENTORHINAL) cortex is medial to the perirhinal (Amaral et al. 1987).

We used the atlas shown in Supplementary Figure S6 to define geographical correspondences in brains and thereby determine areal limits. In a number of cases for the V1 and V2 injections, we made histological verifications of areal limits that did not make significant changes to either the segmentation or the areal FLN values, thereby confirming the efficiency of geographical determination of areal limits for determining the FLN of cortical projections.

In the present study, we report numerous projections to V1, V2, and V4 that have not been previously reported in the principal publications dealing with the anatomy of the early visual areas listed in Table 2. We confirmed in CoCoMac (<http://cocomac.org/>) and complemented by extensive literature searches that all the projections previously unreported were indeed novel.

### Statistical Analysis

All statistical analyses were performed in the R statistical computing environment (R Development Core Team 2010) with additional tools from the MASS and multcomp packages (Venables and Ripley 2002; Hothorn et al. 2008). For each of the 3 injection sites, the mean-standard deviation (SD) relation for the FLNe (proportion of cells from each source area projecting onto the target injection site) was plotted and evaluated with respect to a negative binomial family of models, with the Poisson and geometric distributions considered as extreme special cases. Three models were then compared, the Poisson, the best-fit negative binomial, and the geometric (negative binomial with dispersion parameter equal to 1). The fits for the Poisson case are based on the fact that a Poisson count conditional on

a fixed total is distributed as a binomial with  $SD = \sqrt{\frac{p \times (1-p)}{N}}$ . We set  $N$  equal to  $6 \times 10^5$ , the approximate average total number of extrinsic neurons observed across injections. The negative binomial fits were obtained by simulating counts from a negative binomial distribution for mean values ranging from 2 to  $10^6$  and calculating the mean and SD of the proportions for values of  $\theta$  ranging from 1 to 128. Average curves were based on a spline interpolation of the mean of 20 000 repetitions. From these simulated curves, the values of  $\theta$  and 95% confidence interval were estimated that generated the best fit to the data by a least squares criterion.

### Surface Reconstruction and Atlas Registration

Images of the M129 atlas hemisphere sections (Supplementary Fig. S6) were viewed in Caret and used to trace contours running along the cortical midthickness (layer 4) along with areal identities. A 3D surface was reconstructed, inflated, mapped to a sphere, and registered to the F99 atlas (Van Essen 2002a) using landmark-constrained registration (Van Essen 2004, 2005; Vincent et al. 2009) and a total of 24 landmarks running along geographically corresponding locations (gyri and sulci) in the M129 and F99 hemispheres. Cortical area identities were projected from the M129 section contours to the cortical surface reconstruction and used to trace areal boundaries. Cortical surface nodes enclosed within these areal boundaries were assigned appropriate areal identities. These areal maps and associated colors were deformed (registered) from the M129 to the F99 atlas. Maps of connection strength for V1, V2, and V4 were generated by assigning each surface node the logarithm (base 10) of the average connection strength (FLNe) between the associated area and the target area. A visualization option in Caret allows each connection map to be immediately displayed when any surface node within the target area is selected. The data sets associated with the results shown in Figure 13 are available at [http://sumsdb.wustl.edu/sums/directory.do?id=8280575&dir\\_name=MARKOV\\_CC10](http://sumsdb.wustl.edu/sums/directory.do?id=8280575&dir_name=MARKOV_CC10).

## Results

### FLN Values: Local, Long Distance, and Subcortical

The number of labeled neurons in a given source structure (cortical area or subcortical nuclei) relative to the total number of labeled neurons (for that injection) in the brain (including

the injection area) defines the FLN (FLNt) of that structure (Supplementary Fig. S1) (Falchier et al. 2002). The extrinsic FLN (FLNe) equals the strength of connections with the intrinsic connections excluded.

FLNt was determined in a select number of injected areas (V1, V2, V4, 8, 9/46d, F5, TEO, and 7A). The mean FLNt value of the intrinsic (within-area) connectivity was 79% (68–89%) (Fig. 2A). Because the uptake zone of these tracers is defined and restricted, it is possible to determine the number and spatial location of labeled intrinsic neurons (see technical section of Discussion and Supplementary information). This intrinsic connectivity is highly local. With very small injections, we could accurately measure the local spatial distribution, which revealed an exponential decrease in the density of labeled neurons with distance (Fig. 2B), as shown in previous publications (Barone et al. 2000). The density profiles (Supplementary Fig. S1) were used to measure the spatial extent of intrinsic labeling in the large injections that are required for optimal labeling of the full complements of inputs and their FLN values. This showed that 80% of intrinsic neurons arise within a distance of 1.2 mm from the injection site and 95% within 1.9 mm (Fig. 2C).

Figure 3 compares FLNt values for intrinsic, interareal (short and long distance), and subcortical connections. After the FLNt value of the intrinsic connections, the next largest contribution is from the adjoining cortical areas (i.e., areas that share a border with the injected target area and labeled “short” in Fig. 3), with FLNt values on the order of 16%

(2.5–39%). When only the interareal projecting neurons are considered, the neighboring area has an average FLNe of 80%. The remaining connectivity is shared between long-range corticocortical connections (i.e., “all” the remaining cortical areas beyond the nearest neighbors) with a cumulative FLNt value of 5% (0.8–11%) and subcortical connections with a cumulative FLNt value of 1.1% (0.4–2.8%) (Fig. 3A).

Exploration of the distribution of subcortical inputs shows that the major subcortical input for all 3 visual areas is from the claustrum (0.3% FLNt); projections from the LGN never exceed 0.2% of FLNt (Fig. 3B). The relatively high FLN value of the LGN projection to V2 includes many neurons (30–70%) in interlaminar portions of the LGN as reported previously (Bullier and Kennedy 1983). This stands in contrast to the 4% of the LGN interlaminar cells projecting to V1 (this study).

The injections in parietal, temporal, and frontal lobes showed that the pattern of high local connectivity coupled with a very small subcortical input and weak long-distance connectivity was consistent across many cortical areas (Fig. 3A).

### Cortical Areas Projecting to Areas V1, V2, and V4

Tracer injections in each of these areas revealed a complex and patchy pattern of retrograde label involving dozens of cortical areas and a wide range of labeling densities. These injections confirmed previously reported pathways but also revealed weak or modestly labeled pathways that have not previously been reported. Before discussing the summary tabulations, it is

**Table 2**  
Unknown and known corticocortical projections, with bibliographic references of the known projections to central representations of areas V1, V2, and V4

Target area	Col B	Total of col B	References	Col D	Total of col D
	Documented source areas			Undocumented source areas	
V1	V2, V3, V3A, V4, V4t, LIP, PIP, STP, FST, MST, MT, TEO, PERIRHINAL, TE, TH/TF, CORE, MB, LB, PBc, 8	20	1, 2, 3, 4, 5, 6, 7, 8, 9	DP, 7A, 8B, PGa, IPa	5
V2	V1, V3, V3A, V4, V4t, LIP, PIP, DP, STP, PGa, FST, MST, MT, TEO, TE, TH/TF	16	1, 8, 10, 11	7A, VIP, PO, IPa, PERIRHINAL, MB, LB, PBc, 8	9
V4	V1, V2, V3, V3A, V4t, 7A, LIP, PIP, DP, STP, FST, MT, TEO, TE, TH/TF, 8	16	1, 3, 12, 13, 14, 15	PGa, IPa, PERIRHINAL, MST, ENTORHINAL, INSULA, 9/46d, 9/46v, LB	9

References: 1, Felleman and Van Essen (1991); 2, Boussaoud et al. (1990); 3, Barone et al. (2000); 4, Boussaoud et al. (1991); 5, Falchier et al. (2002); 6, Felleman et al. (1997); 7, Rockland et al. (1994); 8, Rockland and Van Hoesen (1994); 9, Clavagnier et al. (2004); 10, Gattass et al. (2005); 11, Stepniewska and Kaas (1996); 12, Neal et al. (1990); 13, Seltzer and Pandya (1991); 14, Ungerleider et al. (2008); 15, Stanton et al. (1995).

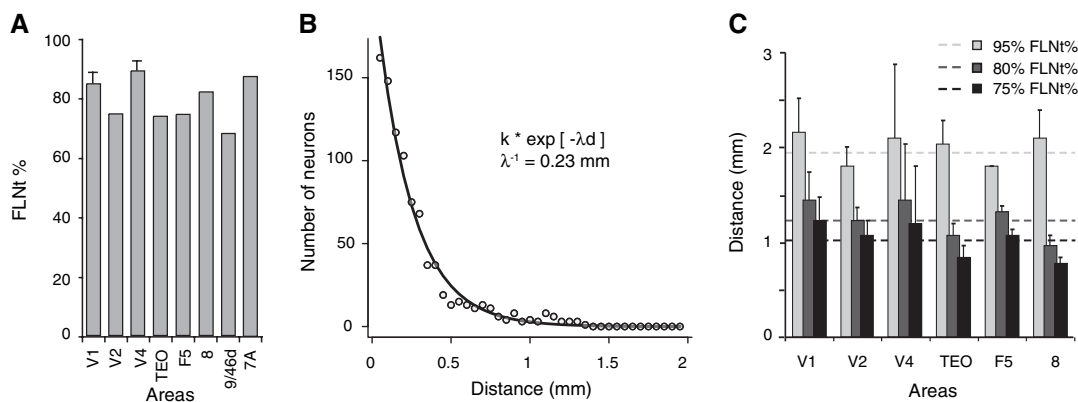


**Figure 2.** Intrinsic and extrinsic connectivity. (A) Intrinsic FLNt values of 9 areas. V1 and V4 are averages for repeated injections. (B) Exponential decay of density of intrinsic neurons with distance following injection in area V1. (C) Distances within which the 3 thresholds (75%, 80%, and 95%) of intrinsic FLNt are attained in 7 injected areas. Dashed lines indicate mean distance at which each threshold is reached. Error bars are SD.

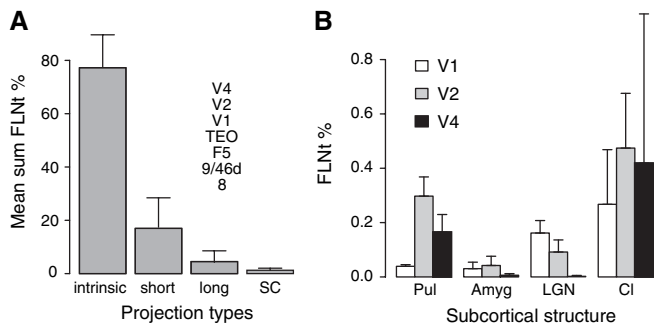


**Figure 3.** FLNt values of cortical and subcortical projections. (A) Mean cumulated FLNt of 4 projection classes. Intrinsic: intrinsic; short: projection from immediate neighbors; long: all the remaining corticocortical projections to the target area; SC: subcortical projections. Error bars indicate the SD. (B) Mean FLNt of the subcortical structures projecting on V1, V2, and V4. Error bars are SD. LGN, lateral geniculate nucleus; Pul, pulvinar nucleus; Cl, claustrum; Amyg, amygdala complex. For area definitions and terminology, see Figure S6 and abbreviations list in Table 4.

useful to illustrate exemplar results for each area in Figures 4–6. Areal boundaries are indicated by black bars, and for clarity, each injected area is shaded gray. In some sections, the label from a restricted region (identified by a black rectangle) of an adjacent section is projected on the section shown.

Results from one of the V1 injections are shown in Figure 4 in a set of horizontal section drawings, with labeled cells shown in red. The injection site in V1 (panels G and H) was in foveal V1, ~2 mm from the V2 border. Retrograde labeling was heavy in several nearby areas (V2, V3, and V4), moderate in a number of more distant areas (e.g., MT and MST in panels C–F), and sparse but unequivocal in numerous other areas in the temporal lobe (e.g., TE and TH/TF in panels I–K) and parietal lobe (e.g., LIP and DP in panels A and B). Labeling in areas not previously reported to be connected with V1 include DP (panel A), PGa (panel G), and IPa (panel I). Among subcortical structures, labeling was notably intense in the claustrum (panel I and H).

Labeling following an injection in area V2, close to the V1 border, is shown in Figure 5 (injection site in panels C and D). As with the V1 example, retrograde labeling is heaviest in nearby areas but includes some label in numerous other cortical areas and also the claustrum (panels L and M). Labeling in areas not previously reported to be connected with V2 include 7A (panel F), VIP (panel G), IPa, MB, (panel L), 8 (panels N and O), PERIRHINAL (panel M), PO (panel A), LB (panel I), and Pbc (panel J).

The exemplar V4 injection (Fig. 6) revealed notably strong retrograde labeling in areas V4t (panels C–E), TE (panels E–L), TH/TF (panels F–I), V3 (panels A and B), and several other areas. Labeling in areas not previously reported to be connected with V4 include PGa (panel G), IPa (panels H and I), MST (panel E), ENTORHINAL, INSULA (panel H and M), 9/46d, 9/46v (panel N and O), and PERIRHINAL (panels J, K, L, and M).

Table 2 lists all 25 pathways identified as providing inputs to each of areas V1, V2, and V4, organized by whether they were previously reported (column B) or unreported (column D). Areas that project to all 3 areas (V1, V2, and V4) include V3, V3A, V4t, MT, FST, TE, TEO, LIP, TH/TF, PERIRHINAL, MST, STP, PIP, DP, PGa, IPa, 7A, LB, and 8. The density of labeling in a given area (e.g., TE) differs markedly in the illustrated sections for the exemplar V1, V2, and V4 injections (Figs 4–6).

However, assessing the magnitude and consistency of these differences requires the quantitative analyses described below.

Some of the newfound projections increase the similarity of the input profile of the early visual areas (see Discussion), but there were exceptions. For instance, the medial belt (MB) and caudal parabelt (Pbc) of auditory cortex project to both V1 and V2 (Figs 4 and 5) but not V4 (Fig. 6), and the core auditory region projects only to V1 (Fig. 4). VIP and PO project only to V2 (Fig. 5), whereas areas 9/46v, 9/46d, INSULA, and ENTORHINAL cortex were found to project only onto V4 (Fig. 6).

### Consistency of Previously Undocumented Projections

The consistency of novel connections was assessed from the repeat injections in areas V1, V2, and V4 (Table 3). Of the 5 newly reported connections to V1, 3 (DP, PGa, and IPa) were found following all 5 injections and had a cumulative FLNe value of 0.01%. For V2, of the 9 newly reported connections, 6 (Perirhinal, 8, VIP, IPa, PO, and MB) were present in all cases and had a cumulative FLNe = 0.09%. For V4, of 9 novel connections having a cumulative FLNe of 1.2%, 4 (Perirhinal, IPa, PGa, and MST) were present in all 3 cases. Overall, 80% of the previously undocumented connections have FLNe values that overlap with those of known connections (Fig. 7). These findings indicate that weak projections are part of a regular connectivity pattern of cortical areas.

### Modeling the Variability of FLN of Projections to Areas V1, V2, and V4

For the quantitative analysis of interareal connections, we used FLNe measurements (FLN restricted to labeled neurons outside of the injected area). Remarkably, the full range of cortical FLN values spans more than 5 orders of magnitude even after the intrinsic connections are excluded.

We analyzed the consistency of individual pathways in order to determine whether a connectivity profile exists. This entailed determining the statistical distribution that best describes the data, including the average connection strength and its variability. Count data are intrinsically heteroscedastic, that is, the SD depends on the mean (Hilbe 2007). In the simplest model of count data, the Poisson distribution, a single parameter determines the mean and the SD equals  $\sqrt{\mu}$  (square root of the mean). Poisson counts conditioned on a fixed total sum,  $N$ , follow a binomial law, in which the SD equals  $\sqrt{\frac{px(1-p)}{N}}$ , and where  $p$  is the mean FLNe value.

Figure 8A displays the SD plotted against the mean of the FLNe values for multiple injections in areas V1 (5 injections and 4 animals), V2 (3 injections and 2 animals), and V4 (3 injections and 3 animals) (FLNe for all V1, V2, and V4 injections are provided in Supplementary Table S1). Axes are scaled logarithmically here (and elsewhere). SD of the FLNe exceeds the prediction for a Poisson-distributed variable (red curve) and for any given pathway is typically about an order of magnitude or less and is therefore considerably less than the total range of connection strengths across different pathways (see Fig. 11 and Supplementary Table S1). Using the Poisson model for statistical tests would lead to increased Type 1 errors (rejecting the null hypothesis when it is true).

The geometric distribution (blue curve) is an alternative model that predicts greater variation than the Poisson model. Under this model, the SD increases as the square root of the mean plus the mean squared, that is,  $\sqrt{\mu + \mu^2}$ . Most data points

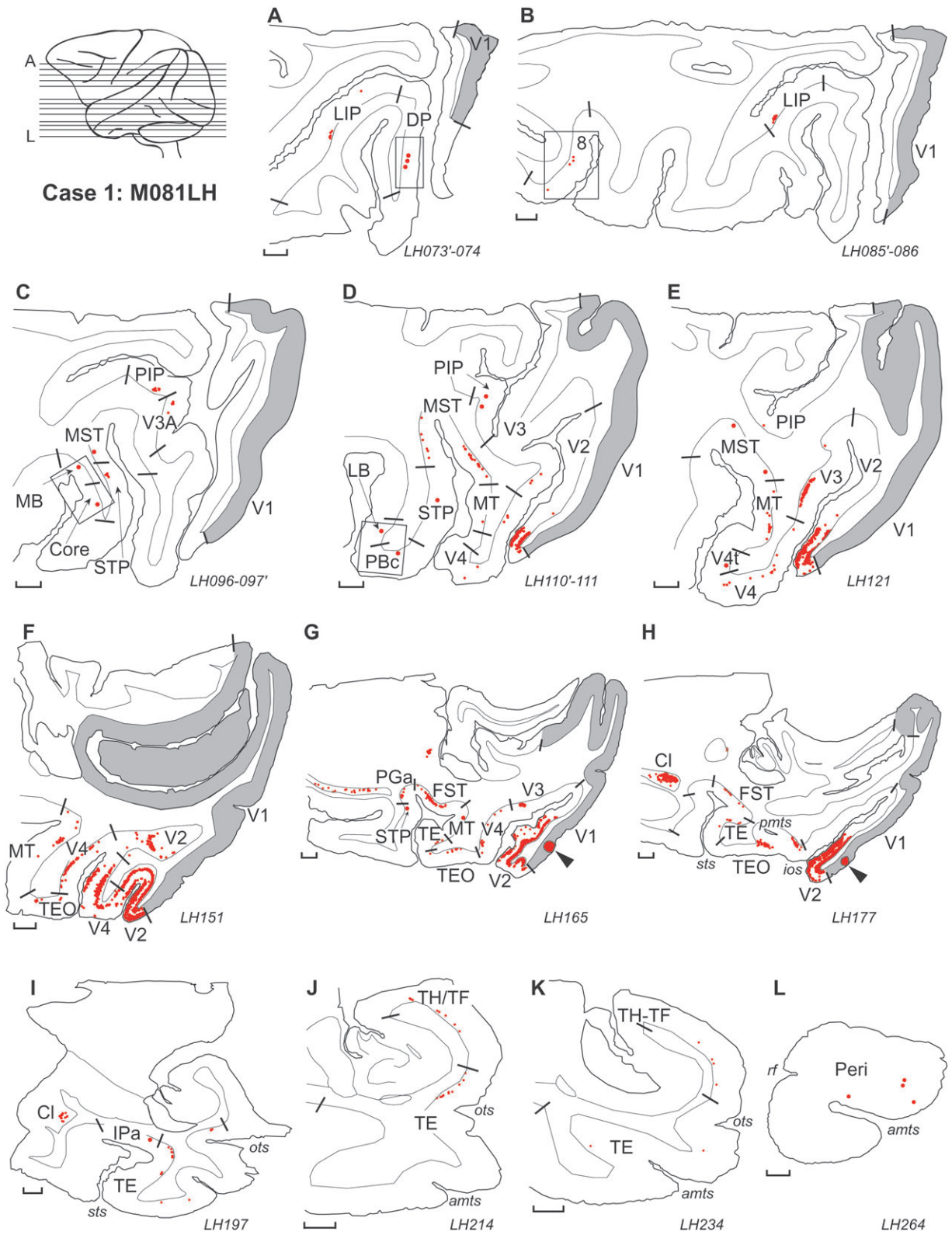


**Figure 4.** Injection in central V1. Upper left: section levels indicated on a lateral view of a cerebral hemisphere. (A-L) Horizontal charts of retrograde-labeled neurons following injection of DY in area V1. Shading indicates the extent of area V1. The injection site is identified as a red point. Projecting neurons are in red. Empty black rectangle indicates neurons from an adjacent section projected on the mapped section.

fall below this curve, suggesting that it predicts too much variability in the data. Using this law would tend to generate Type 2 errors, failing to reject the null hypothesis when it is false. Both the Poisson and the geometric distributions are

extreme examples from the negative binomial distribution family that has proven valuable in the analysis of over-dispersed count data (Lindsey 1999; Venables and Ripley 2002; Hilbe 2007). The negative binomial can be derived as

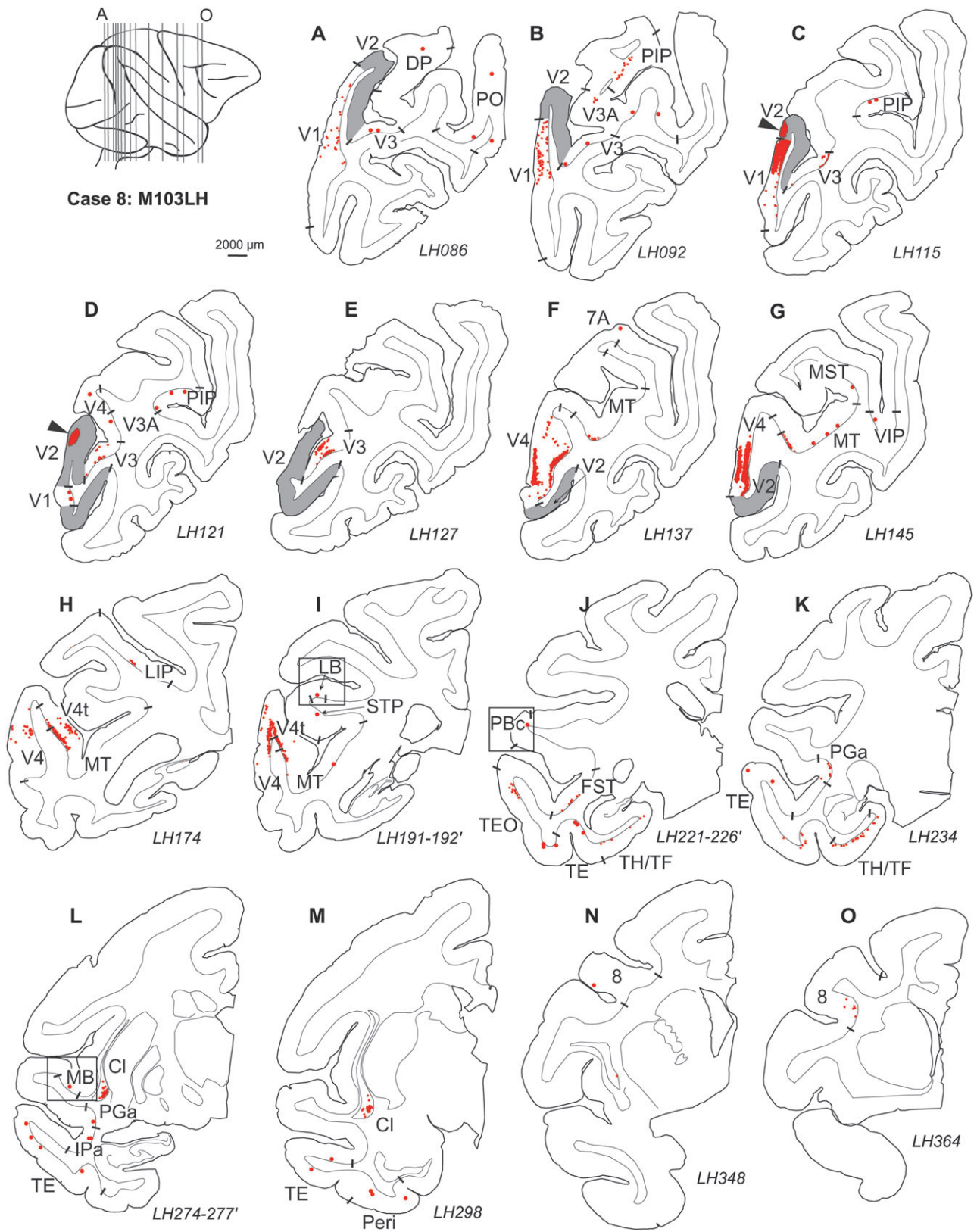


**Figure 5.** Injection in central V2. Upper left: section levels indicated on a lateral view of a cerebral hemisphere. (A–O) Coronal charts of retrograde-labeled neurons following injection of DY in V2. Empty black rectangle indicates neurons from an adjacent section projected on the mapped section.

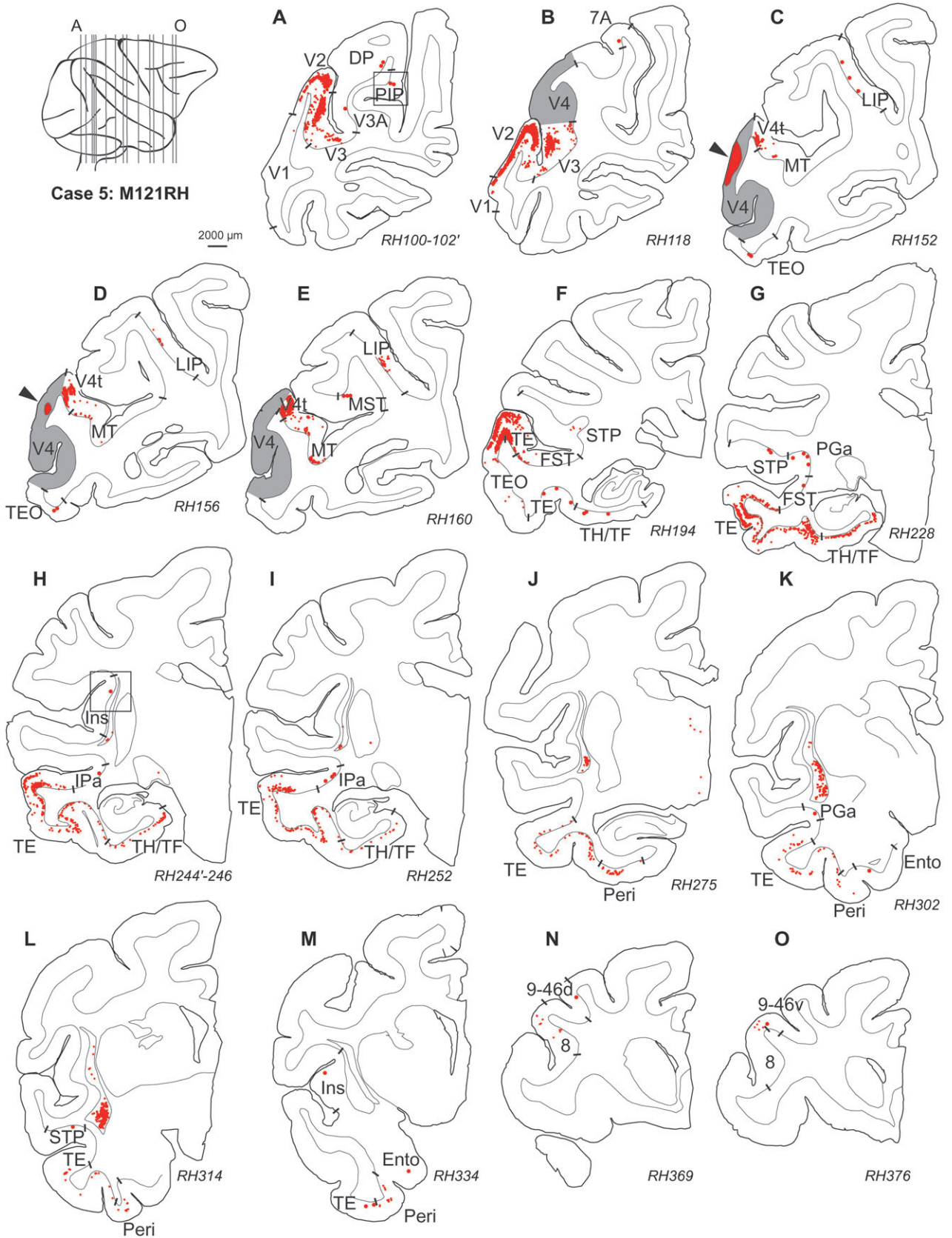


**Figure 6.** Injection in central V4. Upper left: section levels indicated on a lateral view of a cerebral hemisphere. (A-O) Coronal charts of retrograde label neurons following injection of DY in V2. Empty black rectangle indicates neurons from an adjacent section projected on the mapped section.

**Table 3**

Previously undocumented source areas and their average FLNe values to central representations of areas V1, V2, and V4

Source	Target	Number of injections	Geometric mean number neurons and (range)	FLNe	Illustrated in
DP	V1	5 of 5	41 (18, 110)	$3.99 \times 10^{-04}$	Figure 4A
PGa	V1	5 of 5	56 (26, 204)	$5.46 \times 10^{-04}$	Figure 4G
7A	V1	2 of 5	19 (12, 31)	$1.85 \times 10^{-04}$	Supplementary Figure S8C
IPa	V1	5 of 5	21 (8, 68)	$2.05 \times 10^{-04}$	Figure 4I
8B	V1	1 of 5	1 (1, 1)	$9.74 \times 10^{-06}$	Supplementary Figure S8B
PERIRHINAL	V2	3 of 3	139 (78, 200)	$5.43 \times 10^{-04}$	Figure 5M
8	V2	3 of 3	35 (28, 42)	$1.37 \times 10^{-04}$	Figure 5N,O
VIP	V2	3 of 3	28 (11, 88)	$1.09 \times 10^{-04}$	Figure 5G
IPa	V2	3 of 3	8 (1, 27)	$3.13 \times 10^{-05}$	Figure 5L
PO	V2	3 of 3	8 (5, 14)	$3.13 \times 10^{-05}$	Figure 5A
7A	V2	2 of 3	2 (1, 3)	$7.81 \times 10^{-06}$	Figure 5F
MB	V2	3 of 3	2 (1, 3)	$7.81 \times 10^{-06}$	Figure 5L
LB	V2	2 of 3	2 (1, 3)	$7.81 \times 10^{-06}$	Figure 5I
PBc	V2	1 of 3	1 (1, 1)	$3.91 \times 10^{-06}$	Figure 5J
PERIRHINAL	V4	3 of 3	870 (654, 1159)	$9.20 \times 10^{-03}$	Figure 6A,B
IPa	V4	3 of 3	119 (85, 192)	$1.26 \times 10^{-03}$	Figure 6H,I
PGa	V4	3 of 3	21 (2, 75)	$2.22 \times 10^{-04}$	Figure 6K
MST	V4	3 of 3	12 (8, 24)	$1.27 \times 10^{-04}$	Figure 6E
ENTORHINAL	V4	3 of 3	12 (6, 40)	$1.27 \times 10^{-04}$	Figure 6M
INSULA	V4	2 of 3	7 (5, 9)	$7.40 \times 10^{-05}$	Figure 6H,M
9/46v	V4	2 of 3	4 (3, 5)	$4.23 \times 10^{-05}$	Figure 6O
LB	V4	1 of 3	1 (2, 2)	$2.12 \times 10^{-05}$	Supplementary Figure S8A
9/46d	V4	1 of 3	1 (1, 1)	$1.06 \times 10^{-05}$	Figure 6N

a Poisson distribution modified to have a gamma distribution of the mean. A second parameter,  $\theta$ , controls the dispersion of the distribution, with SD equal to  $\sqrt{\mu + \frac{\mu^2}{\theta}}$ . The green curve in Figure 8A indicates the prediction of a negative binomial distribution with the dispersion value for the curve that best fits the data, its 95% confidence interval indicated in the figure. Note that the confidence interval excludes  $\theta = 1$ , which is the geometric distribution. Similar relations were found when areas are considered separately (Fig. 9A–C). A negative binomial is also supported by examination of the symmetry of the distribution of the data. The 95% confidence interval of the average of the median/mean of the FLNe (Fig. 8B, open circle with error bars) differs from the geometric prediction ( $\ln(2) = 0.69$ , red line) and includes the value of the negative binomial model with parameters indicated by the SD/mean relation of Figure 8A (green dashed line in Fig. 8B). This first analysis enables us to restrain the random components of the variability of the data and improves our statistical power.

Armed with this description of the distribution of the data, we can now test the minimum set of factors accounting for the systematic effects on the data from each target area. For each injection site, models of the number of cells from each source area as a function of various explanatory variables were fitted with a generalized linear model (McCullagh and Nelder 1989) with a negative binomial family. The link function was chosen to be logarithmic. The log of the total number of cells counted from each injection was used as an offset or constant component added to the model so that in fact the connection density was modeled (see Materials and methods). Four explanatory variables were evaluated for systematic effects: AREA (a factor with a level for each source area), BRAIN (the individual from which the counts were obtained), DYE (a 2-level factor indicating the tracer used), and HEMISPHERE (the

hemisphere of the injection). For example, if AREA is considered as an explanatory variable, then it is treated as a factor with as many levels as source areas that contained marked cells from the injections in the target areas. A model fit to the data containing only this factor provides estimates of the average FLNe and its variability for each level of AREA.

The selection of the factors and interactions that best described the data was initially based on the Akaike information criterion (Akaike 1993; Venables and Ripley 2002) (AIC), which is defined as follows:  $-2 \times \log(\text{likelihood}) + 2$  (number of parameters used to fit the data). Including more factors and interactions will improve the fit to the data. The AIC introduces a penalty for additional parameters, so that the model with the lowest AIC corresponds to one in which likelihood and numbers of parameters are optimized. The best model, selected in this way, was subsequently verified by evaluating the statistical significance of adding and/or dropping additional terms. The principle hypothesis tested was whether the neural counts across areas were independent of the factor BRAIN.

For all 3 areas with repeated injections (V1, V2, and V4), the model with the lowest AIC included no main effect of the factor BRAIN, subsequently confirmed by likelihood ratio tests (V1:  $F_{3,30} = 2.1$ ,  $P = 0.1$ ; V2:  $F_{1,29} = 0.07$ ,  $P = 0.78$ ; V4:  $F_{2,32} = 0.91$ ,  $P = 0.41$ ). Thus, the simpler models without the BRAIN term were retained. The absence of a main effect of BRAIN implies that quantitative connectivity profiles do not differ significantly across cases, and therefore a robust signature (connectivity profile) exists for each area.

If our analysis overestimated the overdispersion of the data, our model would be less sensitive and might lead to an underestimation of the systematic effect of the factor BRAIN. One possible source of overdispersion could relate to the parcellation of the cortex into individual areas. Figure 9 shows that the observed overdispersion cannot simply be attributed to uncertainties in identifying the limits of cortical areas: regrouping cortical areas into 7 large regions having less uncertainty in their boundaries reduced but did not eliminate overdispersion (Fig. 9D–F). This indicates that overdispersion is an intrinsic feature of the cortex and is not simply a consequence of an experimental error in defining the limits of cortical areas. Importantly, even with this reduction in overdispersion, the factor BRAIN did not contribute a significant improvement to the fit by the source regions themselves (V1:  $F_{4,25} = 0.27$ ,  $P = 0.89$ ; V2:  $F_{2,12} = 1.39$ ,  $P = 0.29$ ; V4:  $F_{2,14} = 1.12$ ,  $P = 0.35$ ). We also considered the possibility that the overdispersion was generated by the weakest projections, which tended to be more variable. However, the results were unchanged when we repeated the analysis with the data set thresholded to eliminate projections with FLNe values less than 0.0001, that is, the factor BRAIN did not contribute a significant improvement to the fit obtained by using AREA alone (V1:  $F_{3,83} = 1.19$ ,  $P = 0.32$ ; V2:  $F_{1,40} = 0.02$ ,  $P = 0.88$ ; V4:  $F_{2,36} = 0.08$ ,  $P = 0.93$ ).

Note, the overdispersion can in part be attributed to interindividual differences because comparing the SDs and means for the 2 cases of multiple injections within an animal (Fig. 10) indicates a smaller dispersion (larger  $\theta$ ).

#### Interareal Connectivity Profiles of Areas V1, V2, and V4

Figure 11 shows the ordered average experimental values and their empirical SDs indicated as error bars for both cortical and subcortical projections to areas V1, V2, and V4. In Figure 11,

the curves are the predictions for an ordered sample from a lognormal distribution with the same number of points as the data points in each area and the same mean and SD as the data. These curves fit the data reasonably well and the points and SDs fall within the estimated 95% confidence interval for an ordered sample from a lognormal distribution (indicated by the gray bands around each curve), suggesting that a lognormal distribution provides a reasonable description of the distribution of FLN values; see also the FLN distribution in Figure 7. For each area, the midpoint of the distribution (half stronger, half weaker) occurs at an FLNe of about  $10^3$ . A few areas on the upwardly curved portion on the far left represent notably strong pathways (FLNe  $> \sim 10^2$ ); a few on the downwardly curved portion on the far right represent notably weak pathways (FLNe  $< 10^4$ ). The majority of pathways are in the middle range ( $10^2 > \text{FLNe} > 10^4$ ). Note that while the distributions of FLN values onto each area are very similar conforming to a lognormal distribution, the orderings are quite different for the 3 areas shown in Figure 11, reflecting the difference in signatures between the areas, which are determined by using the negative binomial as shown below.

After excluding BRAIN as a main factor, the connectivity profile of inputs to each of the areas V1, V2, and V4 was determined (Fig. 12A with V1 in green, V2 in blue, and V4 in

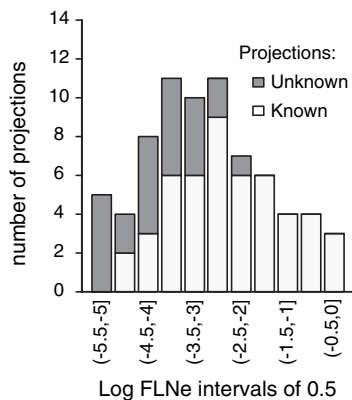


**Figure 7.** FLN distribution of known and unknown connections. Distribution of previously documented (i.e., known) and undocumented (i.e., unknown) projections as a function of projection magnitude (FLNe) at intervals of 0.5 log generated after the injection of areas V1, V2, and V4. Areas and their FLN values are listed in Supplementary Table S1.

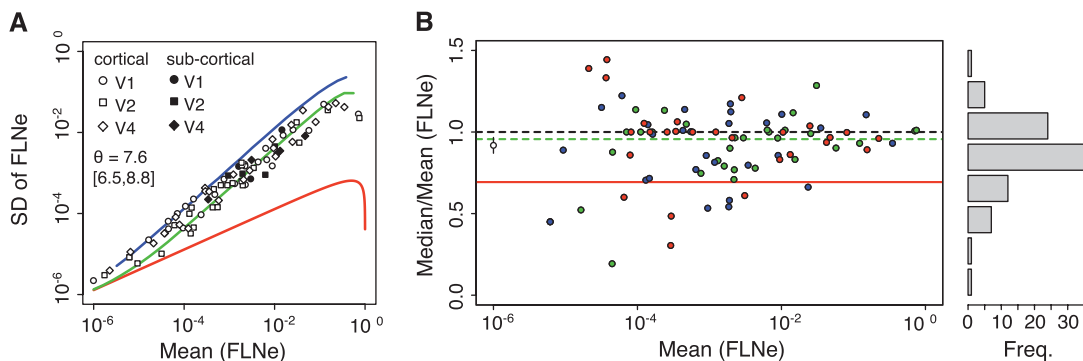


**Figure 8.** Modeling FLN variance. (A) FLNe SD as a function of the mean; green curve, negative binomial;  $\theta$ , dispersion parameter of cortical projections; brackets, 95% confidence interval; blue, geometric distribution; red, Poisson distribution. The estimated SD will tend to be biased for the largest FLNe values as the upper limit of 1 is approached. This accounts for the downturn in the curves of SD vs mean FLNe at large FLNe values. (B) Distribution symmetry as measured by the median/mean as a function of FLNe for area V1; green circle and error bars, mean and 95% confidence interval (0.87, 0.97); red line,  $\log(2)$ , limiting value for geometric distribution; black dashed line, a symmetric distribution; green dashed line (0.96), negative binomial distribution.

red). The profiles shown in Figure 12A include 95% confidence intervals based on the negative binomial model fit to the data. The data are sorted in descending order with respect to the V1 connection weights. The confidence intervals generally are less than an order of magnitude except for the weakest connections, which tend to be more variable. Importantly, the confidence intervals are much smaller than the range of strengths across pathways, thus establishing significant differences between the projections onto a given target area. There is a broad similarity in the strengths of the projections from specific areas to the 3 targets. However, the confidence intervals do not overlap for many pairwise comparisons (e.g., TE projections to V4 are significantly stronger than to V1 or V2). The only case with no overlap of all 3 confidence intervals is area TEO, whose projections are significantly different to V1, V2, and V4. This, plus the complete absence of projections to some target areas for others, indicates an overall different signature of input areas and strengths for each target. Figure 12B shows the profiles of subcortical inputs. These are notable in terms of the small LGN input to V1 (about 1%) and the large projections from the claustrum to the 3 target areas (see also Fig. 3B).

### Surface Maps of FLN

The spatial distribution and strength of connections for each area can be visualized and compared using atlas surface maps (Fig. 13). The cortical areas initially charted on atlas section drawings (Supplementary Fig. S6) were mapped onto a full-hemisphere surface reconstruction (Fig. 13A) and registered to the macaque F99 atlas (Fig. 13B,C). A connectivity matrix (average connection strengths for all source areas with V1, V2, and V4) was linked to these areal maps and visualized using Caret software (Fig. 13D), with a logarithmic scale to display the full range of connection strengths. Visual inspection confirms the preceding assertion that differences in areal connectivity patterns are mainly in the strength of pathways common to all areas rather than in the presence versus absence of connections.

### Discussion

#### Technical Considerations

Several technical considerations could potentially impact the interpretation of our results. These include 1) the possibility of

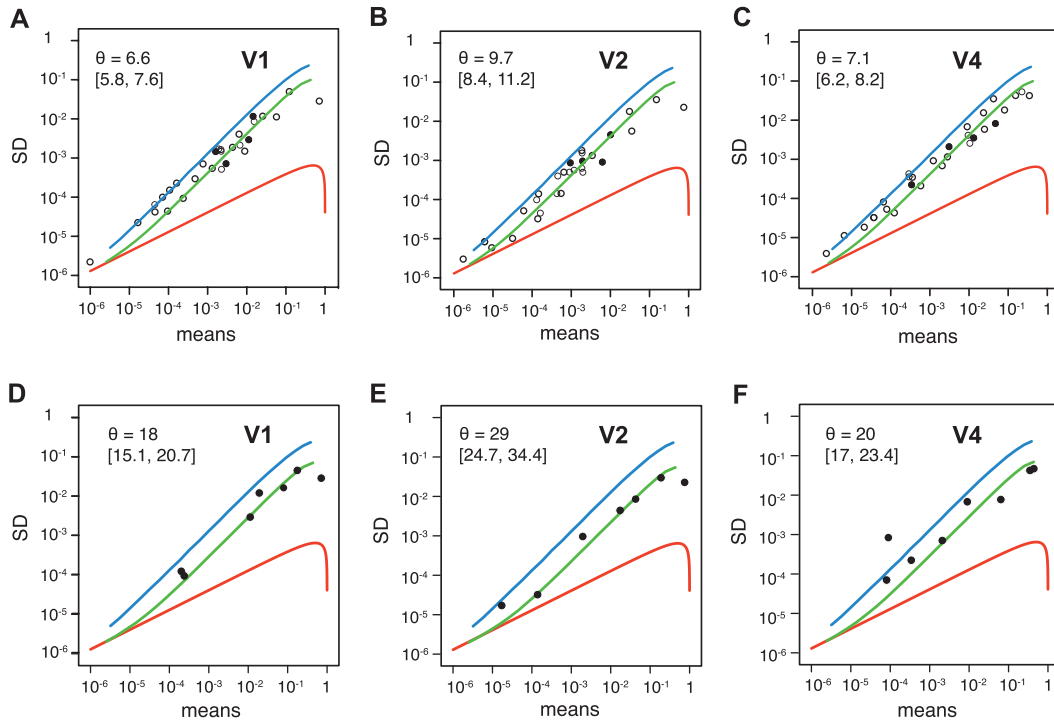


**Figure 9.** Effect of segmentation on variance. (A, B, C) The SD as a function of the mean of the FLNe for the individual projections to V1, V2, and V4, respectively. The estimated overdispersion is similar across each injection site. (E, F, G) The mean/SD relation for the FLNt values pooled into 7 large regions where areas with disputable limits are fused. V1, V2, ventral pathway, dorsal pathway, frontal, subcortical excluding the thalamus. Such pooling that would minimize variability that might occur from errors in segmenting cortical regions produces only minor improvements in the overdispersion of the data. For color codes, symbols, and other conventions, see Figure 8.

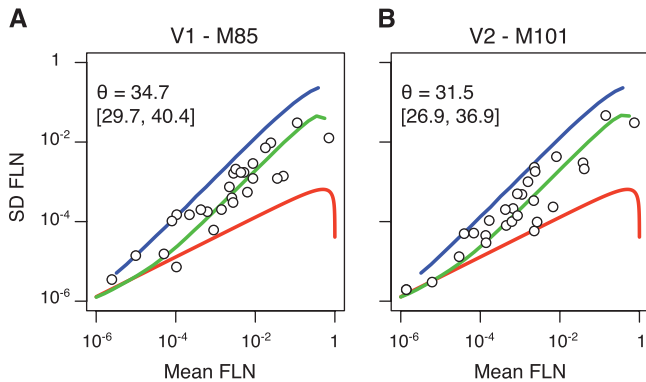


**Figure 10.** Within-individual analysis of variance. SD as a function of the mean of the FLNe. (A) area V1; (B) area V2. For color codes, symbols, and other conventions, see Figure 8.

secondary (transneuronal) uptake of tracer and 2) spread of tracer into white matter or into adjacent cortical areas. As discussed in detail in Supplementary information, we consider it unlikely that any of these issues has a substantial impact on our main findings and interpretations.

#### Previously Unreported Projections to Areas V1, V2, and V4

Since the analysis of Felleman and Van Essen (1991), there has been a major increase in the number of areas reported to project to these areas. These authors reported 7 projections to area V1 (V2, V3, V3A, V4, V4t, PIP, and MT). Successive studies have confirmed these projections and added new ones. Projections to V1 were reported from TEO (Rockland et al.

1994), MST (Boussaoud et al. 1990), TE, TH and TF (Boussaoud et al. 1991), LIP, FST (Barone et al. 2000), STP, CORE, belt and parabelt (Falchier et al. 2002), PERI, and 8 (Clavagnier et al. 2004). The present results confirm these projections and in addition reveal labeled neurons in DP, 7A, 8B, PGa, and IPa. These additional projections increase the similarity of the V1 connection profile to that of areas V2 and V4: projections are reported from DP to both areas (Felleman and Van Essen 1991; Stepniewska and Kaas 1996); PGa is reported to project to V2 (Gattass et al. 2005) and V4 (current study); and 7A is reported to project to V4 (Neal et al. 1990) and V2 (current study); while IPa has not previously been found to project to early visual areas, we find that it projects to all 3 (V1, V2, and V4) in a consistent fashion and involving reasonable numbers of neurons (Table 3).

The Felleman and Van Essen database lists 6 projections to V2 (V1, V3, V3A, V4, MST, and MT) (Felleman and Van Essen 1991). Additional projections were found from V4t, STP, PGa, FST, TEO, TE (Rockland and Van Hoesen 1994; Gattass et al. 2005), V4t, LIP, PIP, DP (Stepniewska and Kaas 1996), and TH/TF (Rockland and Van Hoesen 1994). The present results confirm these findings and in addition finds labeled neurons in 7A, VIP, PO, IPa, PERIRHINAL, MB, LB, PBc, and 8. As with V1, these additional projections to V2 increase the similarity of the profile of this area to that of V1 and V4: perirhinal cortex has been reported to project to area V1 (Clavagnier et al. 2004) as well as V4 (Barone et al. 2000); projections of 8 are reported to V1 (Clavagnier et al. 2004) as well as area V4 (Stanton et al. 1995; Barone et al. 2000).

The Felleman and Van Essen database lists 16 projections to V4 (V1, V2, V3, V3A, V4t, 7A, LIP, PIP, DP, STP, FST, MT, TEO, TE, TH/TF, and 8). Additional projections were reported from

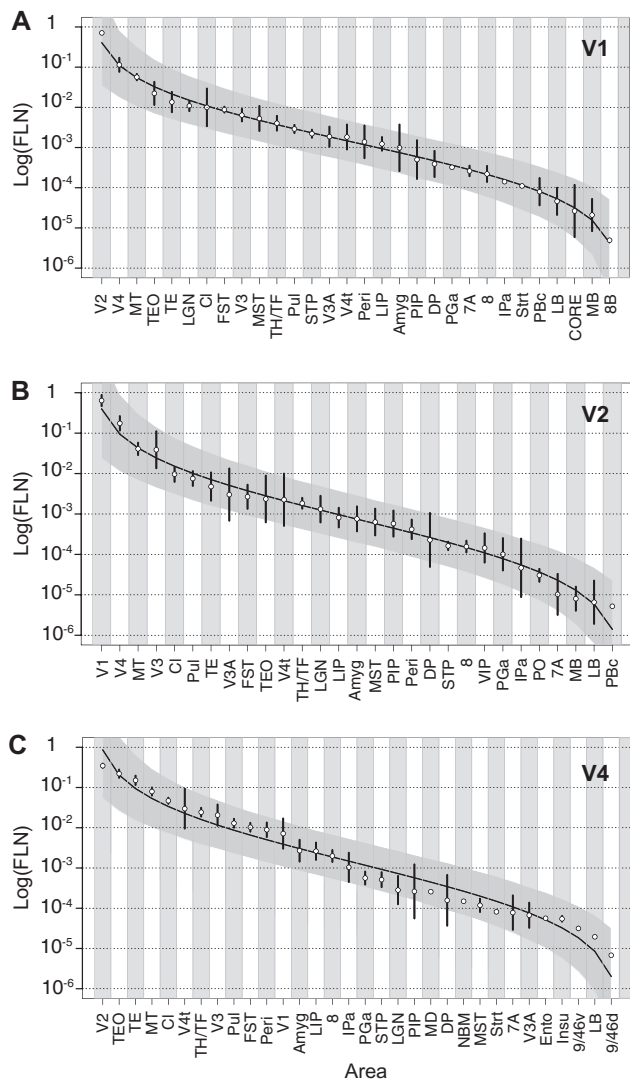


**Figure 11.** Lognormal distribution of FLN values. The observed means (points) ordered by magnitude and SDs (error bars) of the logarithm of the FLNs for the cortical areas projecting on injection sites. (A) V1 ( $n = 5$ ), (B) V2 ( $n = 3$ ), and (C) V4 ( $n = 3$ ). The relative variability increases as the size of the projection decreases. Over most of the range, the variability is less than an order of magnitude. The curves are the expected lognormal distribution for an ordered sample of size,  $n$ , equal to the number of source areas. The gray envelope around each curve indicates the 0.025 and 0.975 quantiles obtained by resampling  $n$  points from a lognormal distribution 10 000 times and ordering them.

7A (Seltzer and Pandya 1991), TE, and 8 (Barone et al. 2000). The present results confirm these findings and in addition finds labeled neurons in PGa, IPa, PERIRHINAL, MST, ENTORHINAL, INSULA, 9/46d, 9/46v, and LB. Here the projection to V4 from MST increases the similarity to V1 and V2 since both areas are reported to receive projections from MST (Boussaoud et al. 1990; Stepniewska and Kaas 1996; Gattass et al. 2005).

Although most of the newly reported projections increase the similarity among projection patterns onto the early visual areas, several have the opposite effect. This includes PO and VIP projections to V2 and ENTORHINAL, INSULA, and 9/46 projections to V4. For all 3 areas, a total of 4 projections could only be detected in one case and each had very low FLN values. Whether these projections are bona fide pathways will be resolved by future studies. Larger injections and higher sampling

rates might reveal these injections to be consistent, and such procedures might have greater sensitivity for detecting additional weak pathways as suggested by others (MacNeil et al. 1997).

### Connectivity Profiles: Local Versus Long Distance, and Subcortical

The small FLNt of the thalamic input to the cortex (Figs 3B and 12) coupled with the high FLNt values of intrinsic connectivity (Fig. 2A) fits with the evidence that local recurrent excitatory networks amplify a numerically sparse feedforward signal (Douglas et al. 1995). For instance, we find that the FLNt of the lateral geniculate nucleus projection onto area V1 is 0.16% (Fig. 3B). This result is consistent with the fact that fewer than 2% of all synapses found in area V1 arise from the lateral geniculate nucleus (Latawiec et al. 2000). The intrinsic FLNt of area V1 that we observe is 85%, consistent with the vast majority of synapses in area V1 originating from local neurons (Binzegger et al. 2004, 2007). The present results showing low subcortical FLN values indicate that this pattern is repeated across the cortex and reveal the high investment of the cortex in local processing. The massive allocation of the neuronal resources of the cortex to local processing and its ongoing patterned activity likewise accounts for much of the brain's energy consumption (Tsodyks et al. 1999; Kenet et al. 2003; Raichle and Mintun 2006). This view of the cortex emphasizes the importance of intrinsic operations, so that the input to a given level of the cortical hierarchy interacts with ongoing activity.

In the connectivity matrix for cat area 17, the vast majority of excitatory synapses in area 17 originate from local neurons, consistent with the intrinsic FLNt of 85% reported here (Binzegger et al. 2004, 2007). Reports from the same laboratory suggest that the synaptic input to a cortical area from a distant area is comparable numerically with the thalamic input (Anderson et al. 1998; Anderson and Martin 2002). These results are compatible with our findings that many different sources converge on area 17 with FLN values equal or inferior to that of the LGN (Fig. 12). This is very relevant to experimental (Stratford et al. 1996; Gil et al. 1999; Bruno and Sakmann 2006) and theoretical (Wang et al. 2010) analyses of how weak cortical inputs can be operationally robust and reliable. Mechanisms that ensure the reliability of the thalamic input to the cortex including synchronization of inputs may also contribute to effective transmission between cortical areas (Tiesinga et al. 2008; Wang et al. 2010).

### Connectivity Profiles: Interareal

An earlier in-depth study of variance suggested that connection strengths are as variable as a geometric distribution and might require the analysis of 10–20 injections to adequately characterize the profile for a given area (Scannell et al. 2000). We demonstrate here that while connectivity strengths do display significant overdispersion, we can exclude the hypothesis that they are geometrically distributed; their variability can be bracketed and their distribution characterized. This characterization has permitted us to obtain reliable estimates of connectivity profiles and their variability using data from 3 to 5 injections.

Overdispersion of the strength of projection from an individual area raises the issue of whether the observed variability reflects genuine individual differences or is intrinsic

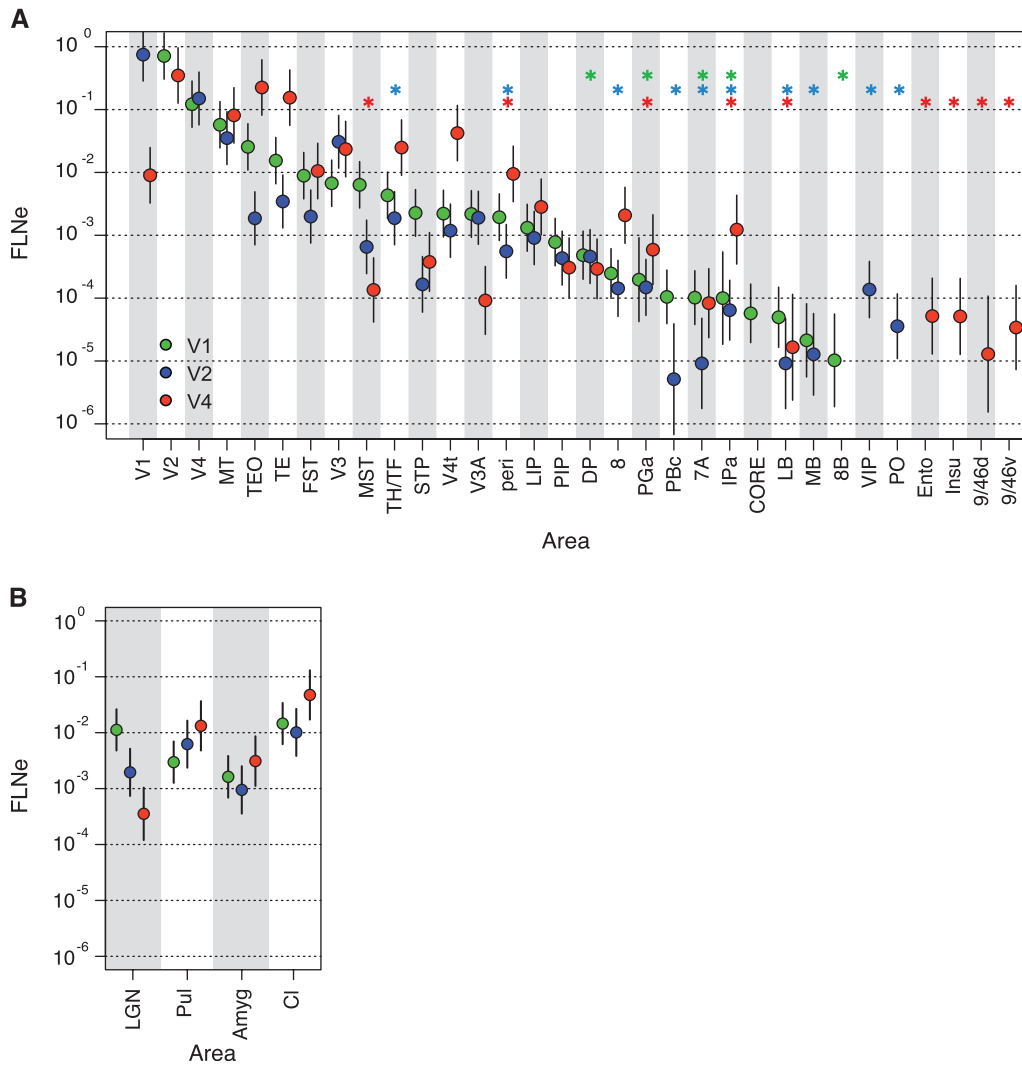


**Figure 12.** Connectivity profiles of areas V1, V2, and V4. (A) Extrinsic FLNe values of cortical projections and 95% confidence intervals for V1 (green), V2 (blue), and V4 (red) as estimated with a negative binomial model. Stars: new previously undocumented projections. (B) Mean log FLNe of subcortical projections with SDs. For other conventions, see Figure 8.

to the technical procedures used. The greater variability observed by Scannell could be attributed to the use of regrouped data from several studies, so that factors such as differences in reliability of the tracers used in the sampling frequency as well as uncontrolled random variations across laboratories may have increased overdispersion. We have shown that the variability of any single projection is considerably less than the range of connectivity weights from the full complement of areas feeding into a given target area, thus permitting the profile to be revealed. The evaluation of the FLN in logarithmic coordinates was key for visualizing a distribution that spans several orders of magnitudes.

The FLN profiles obtained allow us to make 2 important observations. First, connectivity weights span nearly 6 orders of magnitude. In the present study, we report some very weak connections in certain instances including less than 10s of neurons. In 1 or 2 cases, we report just 1 or 2 neurons, which are found in only 1 or 2 cases. However, the numbers of neurons reported reflect only a small fraction of the total number of neurons associated with an area-to-area pathway. If

the entire target area were filled with tracer, the numbers of labeled neurons would be many orders of magnitude greater than the numbers reported here. Second, the distribution of weights to the areas studied here, independent of the areas from which they originate, follows a common pattern, a lognormal distribution. One source of lognormal distributions is via the product of independent random variables (Newman 2005). A simple hypothesis could suppose, for example, that the distribution of weights to a given area arises from a common developmental process of neural growth in which the probability of an axon growing a given distance before making a synapse is the product of randomly varying probabilities that it will stop and synapse at any area along its path. Such a common profile of weights is likely to be the substrate for a common mechanism of information distribution or neural computation by a cortical area. Such a mechanism would suggest a very specific layout of cortical areas and could require some sort of optimization in the location of cortical areas in the 3D structure of the brain (Cherniak et al. 2004; Kaiser and Hilgetag 2006). Interestingly, random outgrowth models have been proposed for the

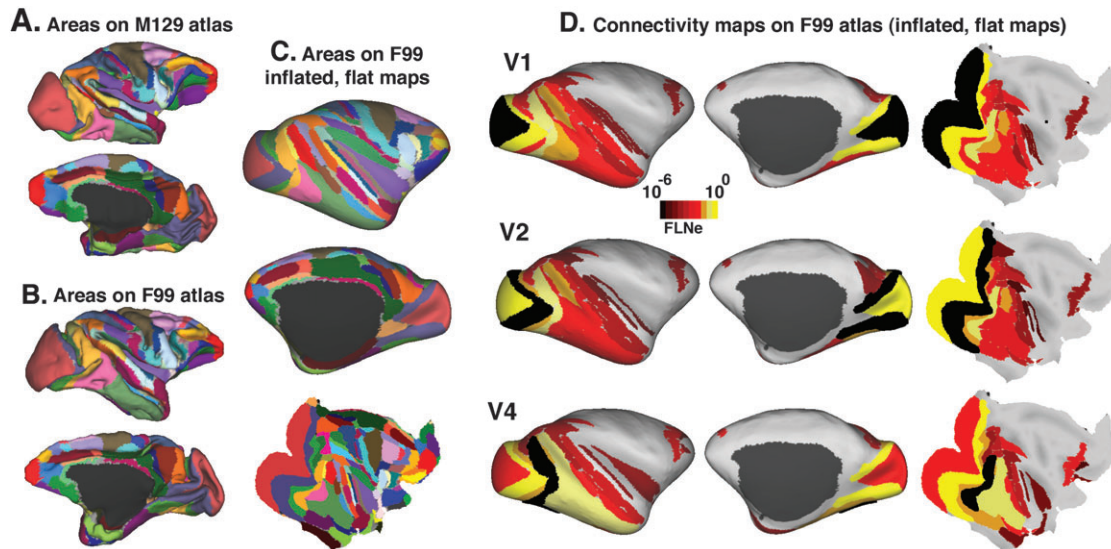


**Figure 13.** Connectivity profiles mapped to a surface-based macaque atlas. (A) A set of 82 cortical areas represented on the M129 right hemisphere reconstructed from section drawings (Supplementary Fig. S6) and displayed on lateral and medial views of the 3D anatomical surface. (B) The same set of areas mapped to the F99 macaque atlas (Van Essen 2002b) and displayed on lateral and medial views of the 3D anatomical surface. (C) The 3D anatomical surface on inflated lateral and medial view of the brain hemisphere and flat map of the areal limits. (D) Average connectivity maps for V1 (top), V2 (middle), and V4 (bottom) displayed on inflated atlas surfaces and a cortical flat maps using a logarithmic scale to represent the range of connection strengths. Injected areas are colored in black. The data sets associated with these results are available at [http://sumsdb.wustl.edu/sums/directory.do?id=8280575&dir\\_name=MARKOV\\_CC10](http://sumsdb.wustl.edu/sums/directory.do?id=8280575&dir_name=MARKOV_CC10).

formation of local connectivity, which if modified to take on board the weight distributions could be extended to concepts of interareal formation (Kaiser et al. 2009)

Interareal connections from neighboring areas may provide inputs that interact with recurrent local connectivity very much in the same way as the feedforward inputs from the thalamus to cortex as described above. However, long-range interareal pathways have FLNe values up to 4 orders of magnitude weaker than the FLNe of the LGN (see Fig. 12A,B). These weak corticocortical connections might contribute to long-range coordination of neuronal assemblies, possibly required for high-level representations (Buzsaki and Draguhn 2004). Interaction of ascending activity with ongoing activity of dense local networks may contribute to multiple brain rhythms, which are in some way controlled by the long-range very sparse connections (Kopell et al. 2000; von Stein et al. 2000; Buzsaki 2007; Lakatos et al. 2008; Uhlhaas et al. 2009). Importantly, these long-range connections are not randomly organized but instead, as shown here, link specific sets of areas with precisely determined connection weights (Table 3) having weights that are typically consistent within a range of 5–8, although some of the weakest projections have a variability exceeding 10-fold (Fig. 12A). The function of the long-range cortical connections may complement nonspecific corticothalamic loops (Llinas et al. 1998). In this respect, cortical-claustrum loops may also be important (Crick and Koch 2005), as an intriguing finding in the present study is that the claustrum provides the strongest subcortical input to the cortex (Figs 3B and 12B).

The lognormal distribution of FLNe values that we observe is a heavy-tailed and heterogeneous distribution that is different from a power law. Lognormal distributions have been reported for a number of biological phenomena, including the nonzero synaptic strengths on single cortical neurons (Song et al. 2005). An interesting parallel can be drawn between interareal (long-range) and intrinsic (local) properties: 1) as we have shown

here, local, intrinsic connectivity shows an exponential decay in density, echoing the decrease in the likelihood of synaptic contact with distance (Braitenberg and Schüz 1998); 2) intrinsic source distributions, just like the extrinsic interareal source distributions, have a patchy character (Yoshioka et al. 1992); 3) lognormal distributions like the one described here for interareal weights have been found for the distribution of synaptic strengths of single neurons (Song et al. 2005). These parallels, at both the cellular and areal levels, suggest that similar logical principles might function over multiple scales.

The present findings increase by nearly 30% the number of projections on to the well-studied visual areas, confirming that an analysis based purely on binary connectivity reveals little specificity. Areas V1, V2, and V4 each receive input from 25 areas. V1 and V2 are distinguished by input from only 4 different areas, meaning that they have a 15% difference in their input profiles. The differences between V1 and V4 and between V2 and V4 are both double that of V1 and V2, indicating a difference of 31% in both cases. If we consider inputs from areas that have no overlapping error bars in Figure 12A as being distinct, then the input differences double and become 31% for V1 versus V2, 69% for V1 versus V4, and 73% for V2 and V4. Hence, these results show that the strength of connection makes an important contribution to defining the connectivity profiles of these areas, despite the high variability of the strengths of the weakest projections. This point is illustrated in Figure 13, where the spatial distribution of inputs to all 3 areas are very similar but where their color-coded FLN values are seen to be very different. The observed projection strength heterogeneity is sufficient to endow specificity to the circuit given the nearly 6 orders of magnitude of the connectivity profile span.

The availability of quantitative macaque connectivity maps plus associated visualization software (Fig. 13) provides a valuable resource for the nascent field of connectomics, which ultimately aims for a comprehensive understanding of local and

**Table 4**

Inset abbreviation list

Index of abbreviations

5	Somatosensory area 5
45	Area 45
46d	Area 46, dorsal part
46v	Area 46, ventral part
7A	Area 7A
8	Area 8
8B	Area 8B
9/46d	Area 9/46, dorsal part
9/46v	Area 9/46, ventral part
Amyg	Amygdala
cal	Calcarine fissure
Cl	Clastrum
Core	Core region of the auditory cortex
DP	Dorsal prelunate area
DY	Diamidino yellow
Ento	Entorhinal cortex
F5	Frontal premotor area F5
F99	Standardized macaque cortical atlas F99
FLN	Fraction of labeled neurons
FLNe	Fraction of extrinsic labeled neurons
FLNt	Fraction of total labeled neurons
FsB	Fast blue
FST	Fundus of superior temporal area
Ins	Insula
IPa	Area IPa
ips	Intraparietal sulcus
LB	Lateral belt
LGN	Lateral geniculate nucleus of the thalamus
LIP	Lateral intraparietal area
Is	Lunate sulcus
MB	Medial belt
MIP	Medial intraparietal area
MST	Medial superior temporal area
MT	Middle temporal area
OPAI	Orbital periallocortex
PBc	Parabelt, caudal part
PBr	Parabelt, rostral part
PERI	Perirhinal cortex (areas 35 and 36)
PGa	Area PGa
Pgm	Parietal area Pg, medial part
PIP	Posterior intraparietal area
PO	Parieto-occipital area
Pos	Parieto-occipital sulcus
ProM	Area ProM
Prost	Prostriata
PUL	Pulvinar
SD	SD
STP	Superior temporal polysensory region
STS	Superior temporal sulcus
Sub	Subiculum
TAa	Area TAa of STP
TE	Area TE
TEO	Area TEO
TH/TF	Area TH/TF
TPO	Area TPO of STP
Tpt	Temporoparietal area
V1	Visual area 1
V2	Visual area 2
V3	Visual area 3
V3A	Visual area 3A
V4	Visual area 4
V4t	Transitional visual area 4
VIP	Ventral intraparietal area

long-distance brain circuitry (Sporns et al. 2005). MR-based neuroimaging methods now enable inferences about long-distance cortical connectivity patterns in humans and non-human primates. However, the technical limitations of these imaging methods can lead to many false positives as well as false negatives when estimating the likelihood of connections (Honey et al. 2009; Johansen-Berg and Behrens 2009). Thus, there is an acute need for independently derived high-fidelity connectivity maps that can serve as references for evaluation and quantitative comparisons. The maps reported here, plus additional data on connectivity for many other areas (Markov

et al. 2011), will be invaluable in this regard. The most direct use will be for comparison with other studies of connectivity in the macaque (e.g., Vincent et al. 2007). Comparisons with human cortex will be facilitated by methods for landmark-constrained interspecies registration between the macaque F99 map used here and the human PALS-B12 atlas (Van Essen 2005) on which R-fMRI connectivity maps (Fox et al. 2005; Fox and Raichle 2007) and many other data have been mapped. Even though there assuredly are major differences in cortical connectivity between macaque and human, many pathways are likely to have been conserved over evolution. Hence, macaque connectivity maps registered to human cortex using known or strongly suspected homologies as constraints will provide an important basis for evaluating in vivo estimates of human connectivity.

In summary, the present results emphasize 2 general features of primate neocortex. First, cortical neurons are massively involved in local circuitry; relatively sparse connections form the main links between processing levels. Second, the strength of a given pathway is consistent across individuals, and the range of strength of connections within an individual extends nearly 6 orders of magnitude, resulting in a stereotyped connectivity profile for each area. Together these findings emphasize the role of strength of connectivity in specifying the connectivity of the cortex and are expected to be important in future and ongoing endeavors directed at elucidating the connectome. Quantitative data providing the relative magnitude of cortical areas projecting to a given target will be invaluable for interspecies comparison of areal connectivity. This issue is important for understanding evolution by allowing distinctions between a remnant of an archaic connection or a strong consistent pathway preserved across species (Palmer and Rosa 2006). Further, FLN values are expected to provide functional insight concerning individual projections. For instance, the newly discovered projections of PERI and amygdala onto the early visual areas have FLN values that are surprisingly high for these very distant projections, thereby lending support to recent cortical theories of inference based on memory prediction (Hawkins et al. 2009).

## Funding

EU-FP6-2005 IST-1583 DAISY to (HK); EU-FP7-2007 ICT-216593 SECO to (HK); ANR-05-NEUR-088 to (HK), National Institutes of Health (R01-MH-60974) to (D.v.E) and in part by Defense Threat Reduction Agency HDTRA 201473-35045 to (Z.T, MMER) and by the Hungarian Bioinformatics MTKD-CT-2006-042794, Marie Curie Host Fellowships for Transfer of Knowledge program to (Z.T).

## Supplementary Material

Supplementary material can be found at: <http://www.cercor.oxfordjournals.org/>.

## Notes

We thank D. Autran, A. Kennedy, S. Zouaoui, J. Beneyton, and A. Batardiere for histological assistance; E. Reid for cortical surface reconstruction; J. Harwell for Caret software development; Donna Dierker for help with analyses; N. Kolomitre, M. Seon, and M. Valdebenito for animal husbandry; M. Brittain and V. Vezoli for administrative assistance. We thank Rodney Douglas and Kevan Martin for critical reading of an early version of the manuscript. *Conflict of Interest:* None declared.

## References

- Akaike H. 1993. Information theory and an extension of the maximum likelihood principle. In: Petrov BN, Csaki F, editors. Second International Symposium on information theory. Budapest (Hungary): Akademiai Kiado. p. 267-281.
- Amaral DG, Insausti R, Cowan WM. 1987. The entorhinal cortex of the monkey: I. Cytoarchitectonic organization. *J Comp Neurol*. 264:326-355.
- Andersen RA, Asanuma C, Essick G, Siegel RM. 1990. Corticocortical connections of anatomically and physiologically defined subdivisions within the inferior parietal lobule. *J Comp Neurol*. 296:65-113.
- Anderson JC, Binzegger T, Martin KA, Rockland KS. 1998. The connection from cortical area V1 to V5: a light and electron microscopic study. *J Neurosci*. 18:10525-10540.
- Anderson JC, Martin KA. 2002. Connection from cortical area V2 to MT in macaque monkey. *J Comp Neurol*. 443:56-70.
- Barbas H, Pandya DN. 1989. Architecture and intrinsic connections of the prefrontal cortex in the rhesus monkey. *J Comp Neurol*. 286:353-375.
- Barone P, Batardiere A, Knoblauch K, Kennedy H. 2000. Laminar distribution of neurons in extrastriate areas projecting to visual areas V1 and V4 correlates with the hierarchical rank and indicates the operation of a distance rule. *J Neurosci*. 20:3263-3281.
- Batardiere A, Barone P, Dehay C, Kennedy H. 1998. Area-specific laminar distribution of cortical feedback neurons projecting to cat area 17: quantitative analysis in the adult and during ontogeny. *J Comp Neurol*. 396:493-510.
- Binzegger T, Douglas RJ, Martin KA. 2004. A quantitative map of the circuit of cat primary visual cortex. *J Neurosci*. 24:8441-8453.
- Binzegger T, Douglas RJ, Martin KA. 2007. Stereotypical bouton clustering of individual neurons in cat primary visual cortex. *J Neurosci*. 27:12242-12254.
- Boussaoud D, Desimone R, Ungerleider LG. 1991. Visual topography of area TEO in the macaque. *J Comp Neurol*. 306:554-575.
- Boussaoud D, Ungerleider LG, Desimone R. 1990. Pathways for motion analysis: cortical connections of the medial superior temporal and fundus of the superior temporal visual areas in the macaque. *J Comp Neurol*. 296:462-495.
- Braitenberg V, Schüz A. 1998. *Cortex: statistics and geometry of neuronal connectivity*. Berlin (Germany): Springer-Verlag.
- Brewer AA, Press WA, Logothetis NK, Wandell BA. 2002. Visual areas in macaque cortex measured using functional magnetic resonance imaging. *J Neurosci*. 22:10416-10426.
- Bruno RM, Sakmann B. 2006. Cortex is driven by weak but synchronously active thalamocortical synapses. *Science*. 312:1622-1627.
- Bullier J, Kennedy H. 1983. Projection of the lateral geniculate nucleus onto cortical area V2 in the macaque monkey. *Exp Brain Res*. 53:168-172.
- Bullier J, Kennedy H, Salinger W. 1984. Branching and laminar origin of projections between visual cortical areas in the cat. *J Comp Neurol*. 228:329-341.
- Buzsaki G. 2007. The structure of consciousness. *Nature*. 446:267.
- Buzsaki G, Draguhn A. 2004. Neuronal oscillations in cortical networks. *Science*. 304:1926-1929.
- Cherniak C, Mokhtarzada Z, Rodriguez-Esteban R, Changizi K. 2004. Global optimization of cerebral cortex layout. *Proc Natl Acad Sci U S A*. 101:1081-1086.
- Clavagnier S, Falchier A, Kennedy H. 2004. Long-distance feedback projections to area V1: implications for multimodal integration, spatial awareness and visual consciousness. *Cogn Affect Behav Neurosci*. 4:117-126.
- Colby CL, Gattass R, Olson CR, Gross CG. 1988. Topographical organization of cortical afferents to extrastriate visual area PO in the macaque: a dual tracer study. *J Comp Neurol*. 269:392-413.
- Conde F. 1987. Further studies on the use of the fluorescent tracers fast blue and diamidino yellow: effective uptake area and cellular storage sites. *J Neurosci Methods*. 21:31-43.
- Crick FC, Koch C. 2005. What is the function of the claustrum? *Philos Trans R Soc Lond B Biol Sci*. 360:1271-1279.
- da Costa NM, Martin KA. 2009. The proportion of synapses formed by the axons of the lateral geniculate nucleus in layer 4 of area 17 of the cat. *J Comp Neurol*. 516:264-276.
- Douglas RJ, Koch C, Mahowald M, Martin KA, Suarez HH. 1995. Recurrent excitation in neocortical circuits. *Science*. 269:981-985.
- Douglas RJ, Martin KAC. 1991. A functional microcircuit for cat visual cortex. *J Physiol Lond*. 440:735-769.
- Falchier A, Clavagnier S, Barone P, Kennedy H. 2002. Anatomical evidence of multimodal integration in primate striate cortex. *J Neurosci*. 22:5749-5759.
- Felleman DJ, Burkhalter A, Van Essen DC. 1997. Cortical connections of areas V3 and VP of macaque monkey extrastriate visual cortex. *J Comp Neurol*. 379:21-47.
- Felleman DJ, Van Essen DC. 1991. Distributed hierarchical processing in the primate cerebral cortex. *Cereb Cortex*. 1:1-47.
- Fox MD, Raichle ME. 2007. Spontaneous fluctuations in brain activity observed with functional magnetic resonance imaging. *Nat Rev Neurosci*. 8:700-711.
- Fox MD, Snyder AZ, Vincent JL, Corbetta M, Van Essen DC, Raichle ME. 2005. The human brain is intrinsically organized into dynamic, anticorrelated functional networks. *Proc Natl Acad Sci U S A*. 102:9673-9678.
- Gattass R, Nascimento-Silva S, Soares JG, Lima B, Jansen AK, Diogo AC, Farias MF, Botelho MM, Mariani OS, Azzi J, et al. 2005. Cortical visual areas in monkeys: location, topography, connections, columns, plasticity and cortical dynamics. *Philos Trans R Soc Lond B Biol Sci*. 360:709-731.
- Gil Z, Connors BW, Amitai Y. 1999. Efficacy of thalamocortical and intracortical synaptic connections: quanta, innervation, and reliability. *Neuron*. 23:385-397.
- Hackett TA, Stepniewska I, Kaas JH. 1998. Subdivisions of auditory cortex and ipsilateral cortical connections of the parabelt auditory cortex in macaque monkeys. *J Comp Neurol*. 394:475-495.
- Hawkins J, George D, Niemasik J. 2009. Sequence memory for prediction, inference and behaviour. *Philos Trans R Soc Lond B Biol Sci*. 364:1203-1209.
- Hilbe JM. 2007. *Negative binomial regression*. Cambridge (MA): Cambridge University Press.
- Hof PR, Morrison JH. 1995. Neurofilament protein defines regional patterns of cortical organization in the macaque monkey visual system: a quantitative immunohistochemical analysis. *J Comp Neurol*. 352:161-186.
- Honey CJ, Sporns O, Cammoun L, Gigandet X, Thiran JP, Meuli R, Hagmann P. 2009. Predicting human resting-state functional connectivity from structural connectivity. *Proc Natl Acad Sci U S A*. 106:2035-2040.
- Hothorn T, Bretz F, Westfall P. 2008. Simultaneous inference in general parametric models. *Biom J*. 50:346-363.
- Johansen-Berg H, Behrens TEJ. 2009. *Diffusion MRI: from quantitative measurement to in-vivo neuroanatomy*. London: Academic Press. p. 490.
- Jones EG, Burton H. 1976. Areal differences in the laminar distribution of thalamic afferents in cortical fields of the insular, parietal and temporal regions of primates. *J Comp Neurol*. 168:197-247.
- Kaas JH, Collins CE. 2001. The organization of sensory cortex. *Curr Opin Neurobiol*. 11:498-504.
- Kaas JH, Hackett TA. 1998. Subdivisions of auditory cortex and levels of processing in primates. *Audiol Neurootol*. 3:73-85.
- Kaiser M, Hilgetag CC. 2006. Nonoptimal component placement, but short processing paths, due to long-distance projections in neural systems. *PLoS Comput Biol*. 2:e95.
- Kaiser M, Hilgetag CC, van Ooyen A. 2009. A simple rule for axon outgrowth and synaptic competition generates realistic connection lengths and filling fractions. *Cereb Cortex*. 19:3001-3010.
- Kenet T, Bibitchkov D, Tsodyks M, Grinvald A, Arieli A. 2003. Spontaneously emerging cortical representations of visual attributes. *Nature*. 425:954-956.
- Kennedy H, Bullier J. 1985. A double-labeling investigation of the afferent connectivity to cortical areas V1 and V2 of the macaque monkey. *J Neurosci*. 5:2815-2830.

- Kopell N, Ermentrout GB, Whittington MA, Traub RD. 2000. Gamma rhythms and beta rhythms have different synchronization properties. *Proc Natl Acad Sci U S A*. 97:1867-1872.
- Kotter R, Sommer FT. 2000. Global relationship between anatomical connectivity and activity propagation in the cerebral cortex. *Philos Trans R Soc Lond B Biol Sci*. 355:127-134.
- Lakatos P, Karmos G, Mehta AD, Ulbert I, Schroeder CE. 2008. Entrainment of neuronal oscillations as a mechanism of attentional selection. *Science*. 320:110-113.
- Latawiec D, Martin KA, Meskenaite V. 2000. Termination of the geniculocortical projection in the striate cortex of macaque monkey: a quantitative immunoelectron microscopic study. *J Comp Neurol*. 419:306-319.
- Lewis JW, Van Essen DC. 2000. Mapping of architectonic subdivisions in the macaque monkey, with emphasis on parieto-occipital cortex. *J Comp Neurol*. 428:79-111.
- Lindsey JK. 1999. *Models for repeated measurements*. Oxford: Oxford University Press.
- Llinas R, Ribary U, Contreras D, Pedroarena C. 1998. The neuronal basis for consciousness. *Philos Trans R Soc Lond B Biol Sci*. 353:1841-1849.
- Luppino G, Hamed SB, Gamberini M, Matelli M, Galletti C. 2005. Occipital (V6) and parietal (V6A) areas in the anterior wall of the parieto-occipital sulcus of the macaque: a cytoarchitectonic study. *Eur J Neurosci*. 21:3056-3076.
- Luppino G, Rizzolatti G. 2000. The organization of the frontal motor cortex. *News Physiol Sci*. 15:219-224.
- MacNeil MA, Lomber SG, Payne BR. 1997. Thalamic and cortical projections to middle suprasylvian cortex of cats: constancy and variation. *Exp Brain Res*. 114:24-32.
- Markov NT, Ercsey-Ravasz MM, Gariel MA, Dehay C, Knoblauch A, Toroczkai Z, Kennedy H. Forthcoming 2011. The tribal networks of the cerebral cortex. In: Chalupa LM, Berardi N, Caleo M, Galli-Resta L, Pizzorusso T, editors. *Cerebral plasticity*. Cambridge (MA): MIT Press.
- McCullagh P, Nelder JA. 1989. *Generalized linear models*. Boca Raton (FL): Chapman & Hall/CRC.
- Mesulam MM, Mufson EJ. 1982. Insula of the old world monkey. I. Architectonics in the insulo-orbito-temporal component of the paralimbic brain. *J Comp Neurol*. 212:1-22.
- Musil SY, Olson CR. 1988a. Organization of cortical and subcortical projections to anterior cingulate cortex in the cat. *J Comp Neurol*. 272:203-218.
- Musil SY, Olson CR. 1988b. Organization of cortical and subcortical projections to medial prefrontal cortex in the cat. *J Comp Neurol*. 272:219-241.
- Neal JW, Pearson RC, Powell TP. 1990. The connections of area PG, 7a, with cortex in the parietal, occipital and temporal lobes of the monkey. *Brain Res*. 532:249-264.
- Newman MEJ. 2005. Power laws, Pareto distributions and Zipf's law. *Contemp Phys*. 46:323-351.
- Olson CR, Musil SY. 1992. Topographic organization of cortical and subcortical projections to posterior cingulate cortex in the cat: evidence for somatic, ocular, and complex subregions. *J Comp Neurol*. 324:237-260.
- Orban GA, Van Essen D, Vanduffel W. 2004. Comparative mapping of higher visual areas in monkeys and humans. *Trends Cogn Sci*. 8:315-324.
- Padberg J, Seltzer B, Cusick CG. 2003. Architectonics and cortical connections of the upper bank of the superior temporal sulcus in the rhesus monkey: an analysis in the tangential plane. *J Comp Neurol*. 467:418-434.
- Palmer SM, Rosa MG. 2006. Quantitative analysis of the corticocortical projections to the middle temporal area in the marmoset monkey: evolutionary and functional implications. *Cereb Cortex*. 16:1361-1375.
- Paxinos G, Huang XF, Toga AW. 2000. *The rhesus monkey brain in stereotaxic coordinates*. San Diego (CA): Academic Press.
- Perkel DJ, Bullier J, Kennedy H. 1986. Topography of the afferent connectivity of area 17 in the macaque monkey: a double-labelling study. *J Comp Neurol*. 253:374-402.
- Petrides M, Pandya DN. 1999. Dorsolateral prefrontal cortex: comparative cytoarchitectonic analysis in the human and the macaque brain and corticocortical connection patterns. *Eur J Neurosci*. 11:1011-1036.
- Preuss TM, Goldman-Rakic PS. 1991. Myelo- and cytoarchitecture of the granular frontal cortex and surrounding regions in the strepsirrhine primate Galago and the anthropoid primate Macaca. *J Comp Neurol*. 310:429-474.
- R Development Core Team 2010. *A language and environment for statistical computing*. R Foundation for Statistical Computing, Vienna (Austria) Vienna (Austria): R Foundation for Statistical Computing Available from: <http://www.R-project.org>.
- Raichle ME, Mintun MA. 2006. Brain work and brain imaging. *Annu Rev Neurosci*. 29:449-476.
- Rockland KS, Pandya DN. 1981. Cortical connections of the occipital lobe in the rhesus monkey: interconnections between areas 17, 18, 19 and the superior temporal sulcus. *Brain Res*. 212:249-270.
- Rockland KS, Saleem KS, Tanaka K. 1994. Divergent feedback connections from areas V4 and TEO in the macaque. *Vis Neurosci*. 11:579-600.
- Rockland KS, Van Hoesen GW. 1994. Direct temporal-occipital feedback connections to striate cortex (V1) in the macaque monkey. *Cereb Cortex*. 4:300-313.
- Saleem KS, Logothetis NK. 2007. *A combined MRI and histology atlas of the rhesus monkey brain in stereotaxic coordinates*. Amsterdam (The Netherlands): Academic Press. p. 326.
- Saleem KS, Price JL, Hashikawa T. 2007. Cytoarchitectonic and chemoarchitectonic subdivisions of the perirhinal and parahippocampal cortices in macaque monkeys. *J Comp Neurol*. 500:973-1006.
- Scannell JW, Grant S, Payne BR, Baddeley R. 2000. On variability in the density of corticocortical and thalamocortical connections. *Philos Trans R Soc Lond B Biol Sci*. 355:21-35.
- Seltzer B, Pandya DN. 1978. Afferent cortical connections and architectonics of the superior temporal sulcus and surrounding cortex in the rhesus monkey. *Brain Res*. 149:1-24.
- Seltzer B, Pandya DN. 1991. Post-rolandic cortical projections of the superior temporal sulcus in the rhesus monkey. *J Comp Neurol*. 312:625-640.
- Song S, Sjöström PJ, Reigl M, Nelson S, Chklovskii DB. 2005. Highly nonrandom features of synaptic connectivity in local cortical circuits. *PLoS Biol*. 3:e68.
- Sporns O, Tononi G, Kotter R. 2005. The human connectome: a structural description of the human brain. *PLoS Comput Biol*. 1:e42.
- Stanton GB, Bruce CJ, Goldberg ME. 1995. Topography of projections to posterior cortical areas from the macaque frontal eye fields. *J Comp Neurol*. 353:291-305.
- Stepanyants A, Martinez LM, Ferecsko AS, Kisvarday ZF. 2009. The fractions of short- and long-range connections in the visual cortex. *Proc Natl Acad Sci U S A*. 106:3555-3560.
- Stephan KE, Hilgetag CC, Burns GA, O'Neill MA, Young MP, Kotter R. 2000. Computational analysis of functional connectivity between areas of primate cerebral cortex. *Philos Trans R Soc Lond B Biol Sci*. 355:111-126.
- Stepniewska I, Collins CE, Kaas JH. 2005. Reappraisal of DL/V4 boundaries based on connectivity patterns of dorsolateral visual cortex in macaques. *Cereb Cortex*. 15:809-822.
- Stepniewska I, Kaas JH. 1996. Topographic patterns of V2 cortical connections in macaque monkeys. *J Comp Neurol*. 371:129-152.
- Stratford KJ, Tarczy-Hornoch K, Martin KAC, Bannister NJ, Jack JJB. 1996. Excitatory synaptic inputs to spiny stellate cells in cat visual cortex. *Nature*. 382:258-261.
- Suzuki WA, Amaral DG. 2003. Perirhinal and parahippocampal cortices of the macaque monkey: cytoarchitectonic and chemoarchitectonic organization. *J Comp Neurol*. 463:67-91.
- Tiesinga P, Fellous JM, Sejnowski TJ. 2008. Regulation of spike timing in visual cortical circuits. *Nat Rev Neurosci*. 9:97-107.
- Tsodyks M, Kenet T, Grinvald A, Arieli A. 1999. Linking spontaneous activity of single cortical neurons and the underlying functional architecture. *Science*. 286:1943-1946.

- Uhlhaas PJ, Pipa G, Lima B, Melloni L, Neuenschwander S, Nikolic D, Singer W. 2009. Neural synchrony in cortical networks: history, concept and current status. *Front Integr Neurosci.* 3:17.
- Ungerleider LG, Courtney SM, Haxby JV. 1998. A neural system for human visual working memory. *Proc Natl Acad Sci U S A.* 95:883-890.
- Ungerleider LG, Galkin TW, Desimone R, Gattass R. 2008. Cortical connections of area V4 in the macaque. *Cereb Cortex.* 18:477-499.
- Van Dijk KR, Hedden T, Venkataraman A, Evans KC, Lazar SW, Buckner RL. 2010. Intrinsic functional connectivity as a tool for human connectomics: theory, properties, and optimization. *J Neurophysiol.* 103:297-321.
- Van Essen DC. 2002a. Surface-based atlases of cerebellar cortex in the human, macaque, and mouse. *Ann N Y Acad Sci.* 978:468-479.
- Van Essen DC. 2002b. Windows on the brain: the emerging role of atlases and databases in neuroscience. *Curr Opin Neurobiol.* 12:574-579.
- Van Essen DC. 2003. Organization of visual areas in macaque and human cerebral cortex. In: Chalupa LM, Werner JS, editors. *The visual neurosciences.* Cambridge (MA): MIT Press. p. 507-521.
- Van Essen DC. 2004. Surface-based approaches to spatial localization and registration in primate cerebral cortex. *Neuroimage.* 23(Suppl 1):S97-S107.
- Van Essen DC. 2005. A population-average, landmark- and surface-based (PALS) atlas of human cerebral cortex. *Neuroimage.* 28:635-662.
- Venables WN, Ripley BD. 2002. *Modern applied statistics with S.* New York: Springer.
- Vezoli J, Falchier A, Jouve B, Knoblauch K, Young M, Kennedy H. 2004. Quantitative analysis of connectivity in the visual cortex: extracting function from structure. *Neuroscientist.* 10:476-482.
- Vincent JL, Kahn I, Van Essen DC, Buckner RL. 2009. Functional connectivity of the macaque posterior parahippocampal cortex. *J Neurophysiol.* 103:793-800.
- Vincent JL, Larson-Prior LJ, Zempel JM, Snyder AZ. 2007. Moving GLM ballistocardiogram artifact reduction for EEG acquired simultaneously with fMRI. *Clin Neurophysiol.* 118:981-998.
- von Stein A, Chiang C, Konig P. 2000. Top-down processing mediated by interareal synchronization. *Proc Natl Acad Sci U S A.* 97:14748-14753.
- Wang HP, Spencer D, Fellous JM, Sejnowski TJ. 2010. Synchrony of thalamocortical inputs maximizes cortical reliability. *Science.* 328:106-109.
- Yoshioka T, Levitt JB, Lund JS. 1992. Intrinsic lattice connections of macaque monkey visual cortical area-V4. *J Neurosci.* 12:2785-2802.
- Young MP. 1993. The organization of neural systems in the primate cerebral cortex. *Proc R Soc Lond B Biol Sci.* 252:13-18.